AD-A087 104 CONNECTICUT UNIV STORRS F/G 11/4
FATIGUE BEHAVIOR OF GLASS FIBER REINFORCED POLYBUTYLENETEREPHTH--ETC(U)
APR 80 A T DIBENETTO DAAG46-78-C-0027
UNCLASSIFIED AMMRC-TR-80-17 NL

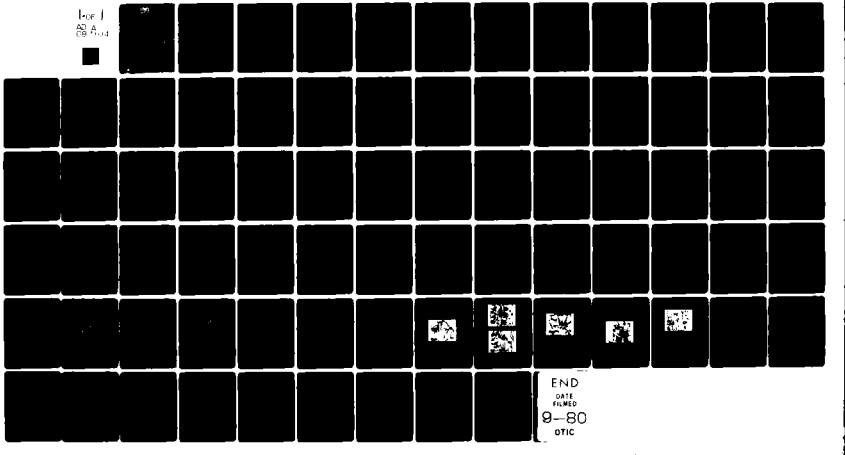

AMMRC TR 80-17

FATIGUE BEHAVIOR OF GLASS FIBER REINFORCED POLYBUTYLENETEREPHTHALATE

April 1980

A. T. DiBenedetto
University of Connecticut
Storrs, Connecticut 06268

FINAL REPORT

CONTRACT NUMBER DAAG-46-78-C-0027

Prepared for

ARMY MATERIALS AND MECHANICS RESEARCH CENTER
Watertown, Massachusetts 02172

The findings in this report are not to be construed as an official Department of the Army position, unless so designated by other authorized documents.

Mention of any trade names or manufacturers in this report shall not be construed as advertising nor as an official indorsement or approval of such products or companies by the United States Government.

DISPOSITION INSTRUCTIONS

Destroy this report when it is no longer needed.
Do not return it to the originator.

UNCLASSIFIED

SECURITY CLASSIFICATION OF THIS PAGE (When Data Entered)

REPORT DOCUMENTATION PAGE	READ INSTRUCTIONS BEFORE COMPLETING FORM
1. REPORT NUMBER: AMMRC TR-80-17	2. GOVT ACCESSION NO.: AD-A087 104
	3. RECIPIENT'S CATALOG NUMBER
4. TITLE (and Subtitle): Fatigue Behavior of Glass Fiber Reinforced Polybutyleneterephthalate	5. TYPE OF REPORT & PERIOD COVERED: Final Report, May 78 - Apr 79
	6. PERFORMING ORG. REPORT NUMBER
7. AUTHOR(s): A. T. DiBenedetto	8. CONTRACT OR GRANT NUMBER(s): DAAG46-78-C-0027
9. PERFORMING ORGANIZATION NAME AND ADDRESS: University of Connecticut, Storrs, Connecticut 06268	10. PROGRAM ELEMENT, PROJECT, TASK AREA & WORK UNIT NUMBERS: D/A Proj.: 1L162105AH8H; AMCMS Code: 62105.11.H8H
11. CONTROLLING OFFICE NAME AND ADDRESS: Army Materials and Mechanics Research Center, Watertown, MA 02131	12. REPORT DATE: April 1980
	13. NUMBER OF PAGES
14. MONITORING AGENCY NAME & ADDRESS (if different from Controlling Office)	15. SECURITY CLASS. (of this report): Unclassified
	15a. DECLASSIFICATION/DOWNGRADING SCHEDULE: N/A

16. DISTRIBUTION STATEMENT (of this Report)

Approved for public release; distribution unlimited

17. DISTRIBUTION STATEMENT (of the abstract entered in Block 20, if different from Report)

18. SUPPLEMENTARY NOTES

19. KEY WORDS (Continue on reverse side if necessary and identify by block number)

Fatigue (mechanics)
Fiber reinforced composites
Polybutyleneterephthalate
Environmental tests

20. ABSTRACT (Continue on reverse side if necessary and identify by block number)

The fatigue behavior of short glass fiber reinforced PBT composites has been investigated under different environmental conditions. Exposure to water at high temperature causes embrittlement, while improved processing and exposure to high humidity cause an increase in ductility. The fatigue life is a function of the environmental conditioning, the stress level of the test and the ductility of the material. The quantity $(\sigma_{max}/\langle\sigma\rangle)^2 \ln t_f$ is independent of environmental

(continued)

DD FORM 1 JAN 73 1473 EDITION OF 1 NOV 65 IS OBSOLETE

SECURITY CLASSIFICATION OF THIS PAGE (When Data Entered)

conditioning and increases with increasing ductility. The total deformation-to-break during fatigue consists of a deformation attributable to cyclic softening (ε_I) and a longer term deformation (ε_{II}) that continues at nearly constant rate until failure occurs. The cyclic softening is associated with cyclic stress-strain characteristics, while ε_{II} is controlled by creep and microcavitational phenomena.

The effect of water treatment on the deformation rate ($\dot{\varepsilon}_{II}$) can be expressed as a master curve for the distribution of $\dot{\varepsilon}_{II}$. It is shown experimentally that the scale of the distribution is a function of the stress level, while the shape depends on the environmental conditioning.

Crack propagation rates in notched plates were measured. The crack propagation behavior was somewhat dependent on the stress history of the material. In the as-received state the crack propagation rate under a given set of conditions tended to decrease significantly and become less sensitive to the imposed stress. After exposure to water, the material became embrittled and the crack propagation rate became somewhat less sensitive to stress history, but much more strongly dependent on the imposed stress. One could not use the crack propagation rates to estimate fatigue life of unnotched materials because of the highly viscoelastic nature of the fatigue process.

longer term deformation

ABSTRACT

The fatigue behavior of short glass fiber reinforced PBT composites has been investigated under different environmental conditions. Exposure to water at high temperature causes embrittlement, while improved processing and exposure to high humidity cause an increase in ductility. The fatigue life is a function of the environmental conditioning, the stress level of the test and the ductility of the material. The quantity $(\sigma_{max}/\langle\sigma\rangle)^2 \ln t_B$ is independent of environmental conditioning and increases with increasing ductility. The total deformation-to-break during fatigue consists of a deformation attributable to cyclic softening (ε_I) and a longer term deformation (ε_{II}) that continues at nearly constant rate until failure occurs. The cyclic softening is associated with cyclic stress-strain characteristics, while ε_{II} is controlled by creep and microcavitational phenomena.

The effect of water treatment on the deformation rate ($\dot{\varepsilon}_{II}$) can be expressed as a master curve for the distribution of $\dot{\varepsilon}_{II}$. It is shown experimentally that the scale of the distribution is a function of the stress level, while the shape depends on the environmental conditioning.

Crack propagation rates in notched plates were measured. The crack propagation behavior was somewhat dependent on the stress history of the material. In the as-received state the crack propagation rate under a given set of conditions tended to decrease significantly and become less sensitive to the imposed stress. After exposure to water, the material became embrittled and the crack propagation rate became somewhat less sensitive to stress history, but much more strongly dependent on the imposed stress. One could not use the crack propagation rates to estimate fatigue life of unnotched materials because of the highly viscoelastic nature of the fatigue process.

TABLE OF CONTENTS

LIST OF FIGURES

LIST OF TABLES

1. INTRODUCTION

Short fiber reinforced plastics are being utilized with increasing frequency as engineering components because of a number of favorable material characteristics. The high specific strength and stiffness with controlled directional reinforcement, good damping properties and the possibility of economic manufacture of intricately shaped components can be considered some of the most important characteristics of these composites.

In recent years, considerable interest has been created in their behavior under monotonic and cyclic loading conditions. While fracture under static load has received much attention, attempts to analyze fatigue failure under cyclic load have been relatively scarce and mainly concerned with rather narrow and specific conditions of testing and materials. Many of the reported investigations have dealt with the statistical variation of the failure process and the fatigue crack propagation mechanism under a restricted set of environmental conditions. The common purpose was to evolve a law with which, using correlation factors such as the stress intensity factor, one could predict lifetime distributions in large populations starting from fatigue crack propagation data. This approach has led to various models, all of which have been demonstrated to be applicable only under restricted conditions.

This research is intended to gather more information on the behavior of short glass fiber reinforced plastics, under different cyclic loading conditions of mean stress level, stress amplitude, frequency and environemnt, and to evolve a model to predict the fatigue behavior from the statistics of the response.

Short glass fiber reinforced polybutylene terephthalate (PBT) has been chosen as a suitable system for this analysis. Among the linear polyesters of terephthalic acid, PBT is currently experiencing rapid growth as an injection moldable engineering thermoplastic. Its high crystallization rate coupled

with good flowability and good thermal stability results in fast holding cycles, which makes for superior processability.

Dimensional stability, due to the low water adsorption, outstanding performance under static and dynamic loading, creep and fatigue resistance, good electrical properties and, finally, the retention of all these characteristics over a broad range of temperatures, humidities and time spans, make it a strong candidate for transportation applications and for electrical and electronic uses (1).

In the first part of this study, the fatigue failure of glass reinforced PBT, under a specific set of environmental conditions, is examined and the fatigue lifetime distributions are related to easily measurable physical properties. In the second part, the effects of the stress ratio R and frequency on the fatigue failure mechanism are investigated. Finally, crack propagation rates are investigated and the data are evaluated as a predictive tool.

II. LITERATURE REVIEW

The Statistical Aspect of Fracture

Scatter in fracture strengths occurs with all materials. The variability of data is often attributed to defects of different sizes (2,3) or to differences in local cross-link densities (3). Both points of view provide an explanation for the scale effect, i.e., the decrease of lifetime with the increase in the volume of the specimen.

Recent experimental results on amorphous and crystalline polymers (4,5) indicate that primary carbon bonds fracture throughout the specimen. When a critical concentration of broken bonds is reached, submicroscopic cracks increase in concentration and grow until fracture occurs. The local concentration of broken bonds at the tip of a growing notch was also found to be the same as the average global concentration necessary to cause fracture (6). This implies that there is a critical local concentration of broken bonds necessary

to cause local failure which could be initiation of a local flaw or the extension of an existing crack. Since fracture of a bond is probabilistic in nature, there exists a variability in the time of fracture even in specimens that are identical at the molecular level. The spatial distribution of weak sites is a contributing cause of the variability in failure times. In random fiber composites, the distribution of critical flaws due to the poor material uniformity determines the statistical variability of the failure response. A stochastic model, thus, has to be adopted in order to extract information on the relations between the statistics of the fracture process and the mechanical and environmental history of the structure.

Brittle fracture originates in highly localized regions where stress is concentrated at submicroscopic flaws. Fracture of a specimen at a given level of stress depends on the statistical expectations of encountering a critical (or weakest) flaw having the specified strength. If flaws are distributed at random throughout a population, the distribution of strengths is statistically related to the distribution of largest flaws appearing throughout the population. This model is identical to the generalized asymptotic theory of extreme values (7). For samples consisting of n elemental volumes having a probability density function of elemental strength $f(\sigma)$ (i.e. $f(\sigma)d\sigma$ = fraction of elements having a strength between σ ($\sigma + d\sigma$)) and cumulative distribution of elemental strengths $F(\sigma) = \int_o^\sigma f(\sigma)d\sigma$, the distribution of smallest values of σ (i.e. the fraction of specimens with a strength between σ and ($\sigma + d\sigma$)) is given by:

$$g_n(\sigma) = nf(\sigma)(1 - F(\sigma))^{n-1} \tag{1}$$

and the cumulative distribution of sample strengths is given by:

$$G_n(\sigma) = \int_o^\sigma g(\sigma)d\sigma = 1 - (1 - F(\sigma))^n \tag{2}$$

This is the probability of encountering a specimen with a strength equal to or less than σ. For the case of fracture, the elemental probability function $f(\sigma)$

is unknown since the random variable σ cannot be measured directly except for the extreme value itself (i.e. the fracture stress of the material).

A model for the function $f(\sigma)$ has been developed by Weibull based on experimental data on the cumulative distribution of sample strengths $G(\sigma)$ (8,9). A two parameter version of the Weibull function is:

$$f(\sigma) = \frac{\sigma}{\sigma_o} \left(\frac{\sigma}{\sigma_o}\right)^{\alpha-1} \exp - \left(\frac{\sigma}{\sigma_o}\right)^{\alpha} \tag{3}$$

which results in a cumulative distribution of sample strengths given by:

$$1 - P(\sigma) = G(\sigma) = 1 - \exp - n\left(\frac{\sigma}{\sigma_o}\right)^{\alpha} \tag{4}$$

where σ_o and α are constants and n is the number of elemental volumes in the material. (For a population with specimens of fixed volume, n is constant and may be combined with the constant σ_o.). This type of equation is widely used to characterize the variability of strength in fiber reinforced composites (10-17).

The results of fatigue tests can also be characterized by the statistics of extreme values. The specimens that fail under a given stress amplitude at various numbers N of load cycles may be considered as forming a group of the weakest specimens out of a large population of samples. The distribution of N among this subpopulation may therefore be described by a Weibull function of the form (18):

$$1 - P(N)_S = G(N)_S = 1 - \exp - \left(\frac{N}{N_o}\right)^{\alpha_f} \tag{5}$$

where G(N) is the cumulative probability of encountering a specimen with a life of N cycles or less under a stress of amplitude S. The parameters N_o and α_f are constants.

Equations 4 and 5 are only two of a variety of cumulative distribution functions that might be used to describe the strength and fatigue life distributions of fiber reinforced materials. More complex forms must be used

when factors such as a lower limiting strength, endurance limits, biomodal elemental probability distributions or induction times for crack nucleation must be considered.

Regardless of the exact functional forms for the cumulative distribution equations, it is likely that if both breaking strengths and cycles to failure can be described as Poisson processes, one should be able to find a functional relationship between the two quantities at equiprobability points in the respective distributions, i.e.:

$$(N)_s = f(\sigma_b) \ @ \ P(N)_s = P(\sigma_b) \tag{6}$$

This idea will be used to develop a single "master-curve" of fatigue-life versus breaking strength for a given population of material. The master curve will then be used to estimate changes in fatigue lifetime caused by environmental degradation.

Fatigue in Polymers and Composites

Several modes of fatigue failure are observable in glassy polymers: creep, brittle failure that involves craze initiation and crack breakdown (true mechanical failure), thermal softening, or a combination of effects. The polymer fatigue behavior is controlled by both the material variables and the nature of the fatigue test. Some of the material variables identified include the toughness of the polymer, degree of crystallinity, relative importance of homogeneous versus heterogeneous deformation (including the role of crazing), and the location of various damping peaks relative to the time and the temperature of the fatigue test.

The test conditions themselves also have a major effect on the fatigue performance of a given polymer. For example, thermal effects are enhanced by thick specimen dimensions, by the absence of notches, by the use of high strain rates, large strains and by high frequencies.

In cyclic fatigue of ductile polymers, a cyclic softening process is always present which is independent of the specific deformation mechanism acting during fatigue (19). Different failure mechanisms or testing variables do not affect this overall response in kind but only in degree. Only at very low strain levels can one ignore cyclic softening in semicrystalline, amorphous and composite polymeric materials.

This decrease in the resistance to nonelastic strain, as cyclic deformation proceeds, is a homogeneous mechanical phenomenon unrelated to total effects, such as crack propagation, but connected primarily to the anelastic and viscoplastic components of the strain. If we refer to a strain-controlled fatigue test, four different regions can be observed during the softening process:

1) An initial, or incubation region, usually very small and not always present, characterized by a macroscopic and stable cyclic softening
2) A transition stage, in which the peak stress decreases rapidly
3) A cyclic steady state region where a new stable state is attained and the greatest part of the fatigue process is spent
4) A region of crack propagation terminated by fatigue fracture.

For polymers with relatively nonhomogeneous microstructures, i.e., composites containing a high volume fraction of the second phase, the third region is not truly stable and a gradual softening occurs throughout the fatigue life after an initial macroscopic softening. In addition, the first stage, i.e., the incubation region, is usually absent in fiber reinforced composites. It is important to note that the softened state represents a new stable state

of the material since recovery processes are very slow at ambient temperature and zero stress.

Cracks can initiate during the very early cycles of fatigue even in unnotched samples of short fiber composite materials since they invariably contain flaws of some kind due to the fabrication process. Two modes of interest may be noted in the mechanical fatigue response of a glass fiber reinforced plastic (20):

- When the applied cyclic stress is high enough to be within the fiber strength distribution, there is a high fiber failure density in the first cycle. Failure then occurs by the coalescence of local fiber breaks which then propagate to connect other such regions until the specimen fails catastrophically.
- At intermediate levels of cyclic stress, microcracks are initiated in the matrix phase and propagate during cycling until delamination begins.

Several models have been proposed for fatigue crack growth. J. Williams (21) assumes that the effect of cycling is to reduce the craze stress to some proportion of the original value depending on the degree of unloading. Successive loadings result in growth of the craze with a corresponding increase in crack opening displacement. At some critical value of this displacement, crack growth occurs and the rate of growth is related to the applied stress intensity factor. Since the craze at the crack tip in a stressed polymer is a system of interconnected voids in which the ligaments of material between the voids provide the strength of the craze, it is reasonable to expect that some of the ligaments will be damaged, i.e., the craze stress will be reduced, by cyclic loadings and unloadings.

From fatigue crack growth studies on PVC sheets, N.J. Mills and N. Walker (22) have concluded that crack growth occurs discontinuously once every few

hundred cycles while craze growth occurs continuously at the crack tip. In addition, they show that except at very high strains, the crack does not jump the full length of the existing craze when it grows, but it advances only a fraction of the craze length. This mechanism is confirmed by observations of the fatigue fracture surfaces which show striations regularly spaced, each band corresponding to the incremental advance of the crack. Similar results have been reported by other investigators (23,24). Kambour (25) emphasizes, as another peculiar aspect of craze deformation for fatigue fracture, the relaxation behavior associated with the yield of material in and out of the craze as the load is alternately increased and decreased. A role for hysteretic heating, in a small volume element at the crack tip, has also been hypothesized (26,27) but the overall mechanism is still clearly different from thermal failure which is observed under high frequency and for high load test conditions.

Transition from brittle cracking to thermal softening has been found to depend on cyclic wave form and frequency, mean stress, load amplitude, and surface area to volume ratio of material (28). Analytical relationships have been developed which reveal this softening mechanism to be related to the loss compliance of the material, the stress level, test frequency and thermal properties of polymers (29).

The internal damping characteristics of polymers have also been reported to undergo changes during cyclic loading, probably due to a non-uniform volume contraction induced by fatigue loading in the structure of the material (30).

R.J. Crawford and P.P. Benham (31) have found that the stress for change-over from thermal softening to mechanical failure, for some common thermoplastics (acetal, PMMA, polypropylene and unfilled polytetramethylene terephthalate PTMT), is related to the cyclic frequency and surface area to volume ratio. The effect of a sharp notch has been found to reduce the thermal effect so that, for example, fatigue failures are produced in polypropylene

and PTMT under stresses which would only produce thermal failure in unnotched material.

Fatigue Crack Growth Laws

A number of fatigue crack growth laws have been proposed, most of them based on the application of linear elastic fracture mechanics principles to the fracture analysis of elastic materials. The widely known crack propagation equation, due to Paris (32), has been successfully applied to the analysis of cyclic crack growth in many materials for elastic or quasielastic situations:

$$d(2a)/dN = c\ (\Delta K)^m \qquad (7)$$

where 2a is the crack length, N is the number of cycles, ΔK is the range of the stress intensity factor, $\Delta K = K_{max} - K_{min}$, while c and m are numerical constants dependent on the material tested, the environment and the conditions of cyclic loading.

Many authors have reported a strong FCP dependence on mean stress intensity K_m as well as on ΔK (33-38). From fatigue tests on PMMA and PC center-notched plate specimens, Radon and Culver (33,34,36) have reported a distinct influence of both K_m and ΔK on crack growth rates and a FCP increase with increasing values of K_m, other testing conditions being equal. The crack growth rate was found to increase with increasing values of λ, where $\lambda = (K_{max}^2 - K_{min}^2) = 2\Delta K \cdot K_m$. From their observations they have also concluded that fatigue crack growth can be divided into three different stages, each one differently affected by mean stress and stress range.

Sauer and co-workers (35) have investigated the fatigue behavior of PS both in completely reversed axial stress and at various superimposed mean stress values. By varying the mean stress with a fixed value of ΔK, the logarithm of the fatigue life has been found to decrease linearly with

increasing mean stress over the stress range investigated. Conversely, by keeping the peak stress constant while varying the mean stress, the specimen fatigue lifetimes have been found to increase steadily with increasing mean stress. At high values of the imposed stresses, they have reported fracture characteristics very similar to those of static fracture. The endurance limit, i.e., the stress amplitude value at which the fatigue lifetime is 10^7 cycles or greater, has been found to be a strong function of the mean stress. On the basis of completely reversed loading tests, they also demonstrate the deleterious effect on fatigue lifetime of stress cycling into compression, probably due to a certain amount of sharpening of the crack tip during compression.

From all these observations, it can be deduced that FCP behavior of polymers is strongly influenced by the stress amplitude, the mean stress and maximum stress, the more effective depending on the specific loading conditions. At very low mean stresses, the stress amplitude effect prevails and becomes more important for strain sensitive materials. At medium values of the mean stress, the crack growth rate seems equally dependent on ΔK and K_m, while, at very high mean stresses, creep effects dominate and the total FCP rate may be viewed as consisting of the summation of fatigue and creep. In this case, crack growth rate is mainly regulated by the K_m value. Stress amplitude and peak stress also affect the rate of energy dissipation, and, at very high values, thermal softening may occur depending on the loss compliance and the heat transfer characteristics of the sample.

Environmental Effects

The effects of environment on the mechanical behavior of fiber reinforced epoxies have been extensively reviewed by Ishai (39,40). Ishai has suggested that there are two effects of water penetration on composite strength, one the reduction of interfacial toughness and, consequently, of composite tensile

strength and second stress-environment induced damage such as matrix cracking, interfacial debonding and chemical deterioration of the glass fibers with irrecoverable weight loss with time. The weight loss of GRP specimens under hot water exposure has been attributed to a temperature dependent attack on the glass fiber surface and the interfacial coupling agent phase by the water, with consequent leaching and removal of the glass constituents. Many other authors have reported similar degradation effects on the mechanical properties of composite materials (41-43). Y.W. Mai (43) has investigated the fracture behavior of short glass fiber reinforced polystyrene for three environmental conditions: air, water, and hot water exposure at 363°K. The glass filled composites have, for a given temperature, lower resistance to crack propagation when tested in water and when subjected to hot water absorption and subsequent drying. In this case too, the fracture toughness degradation has been explained as the result of both a reversible and irreversible damage due to water penetration.

III. EXPERIMENTAL PROCEDURES

Materials

Approximately 400 injection molded ASTM standard dog bone specimens of glass fiber reinforced polybutylene terephthalate composites containing 20 (±1) percent by volume glass fiber were obtained from the Hooker Chemical Company. In addition, several pounds of the same material in pellet form were obtained in order to prepare fracture toughness specimens. The specimens were annealed under vacuum for 48 hours at 150 C. One hundred sixty of these were then placed in an environment of air at 23°C and 55 percent relative humidity, another 80 in air at 23 C and 95-100 percent relative humidity, another 80 in boiling water for 192 hours and the remaining 80 in 70 C water for 504 hours. The test bars came from four different injection molding runs. Preliminary stress-

strain data indicated that from a statistical point of view, three of these runs (of 100 specimens each) produced identical populations. The fourth run of 100 specimens produced a population with slightly higher ductility and strength in the as-received state and subsequently proved to have a greater fatigue life in the as-received state. These differences, however, disappeared after long term exposure to 70 C or boiling water. The five populations used in this study are designated in the following manner:

1-RH55	High strength population - as received
2-RH55	Normal population - as received
3-RH100	Normal population - exposed to 100% relative humidity
4-BW192	Normal population - exposed to boiling water for 192 hours
5-HW504	Normal population - exposed to 70% water for 504 hours.

Tensile Testing Procedure

The stress-strain behavior of the five populations was established by testing about 15-20 samples per population on an INSTRON 1230 electrohydraulic closed-loop testing system. Experiments were conducted at a crosshead rate of 0.2 in./min. at 23 C and 40 percent humidity (normal room conditions). The ultimate strength, the elongation-to-break, the initial tangent modulus and the modulus of toughness were calculated for each specimen.

Fatigue Testing Procedure

A sinusoidal oscillation, at a fixed frequency of 10 Hertz and at a constant ratio of minimum to maximum stress equal to 0.67 (i.e., $R = \sigma_{MIN}/\sigma_{MAX} = 2/3$), was employed using the INSTRON 1230 testing machine.

Each specimen was subjected to cyclic tension under selected maximum and minimum values of load. Different stress levels L (i.e. $L = \sigma_{MAX}/\langle\sigma_b\rangle$) were used for different sets of specimens, 90% of the breaking strength being the maximum level chosen. The load levels were constantly monitored on an oscilloscope during each run.

From the fatigue tests, the time to break of each sample was determined by means of an automatic cycle counter and the rate of strain during fatigue, in terms of change in the strain level per cycle of deformation, was determined by measuring the maximum axial displacement as a function of time.

Effect of Frequency

In order to examine the effect of frequency on the fatigue behavior, specimens from the population 2-RH55 were tested under cyclic loading conditions between frequencies of 1 and 45 cycles per second (Hz). The fatigue tests were conducted in fluctuating tension at different maximum stress at a constant stress ratio R equal to 2/3.

The strain rate was monitored as a function of frequency whose range was scanned several times for each specimen until steady values for the strain rates were obtained, i.e., until the same strain rate was obtained at the same frequency level during two consecutive scans.

Effect of Stress Ratio

The cyclic behavior of short glass fiber reinforced PBT under different amplitudes of load (i.e. different ratios of minimum to maximum stress, R) was also examined. The measurements were performed on specimens from the population 2-RH55 at a fixed frequency of 10 Hertz, with stress ratios ranging from 0.42 to 0.92 and at two different values of the maximum stress level L. Strain rates were reported at different values of the stress ratio. The whole stress ratio range was scanned several times until steady strain rate values were obtained.

Measurement of Crack Propagation Rate

Crack propagation tests were made using 2.24 inch wide compact tension specimens (44) made from extruded sheets which were then laminated and compression molded to form one-half inch thick specimens. Pre-notched specimens were precalibrated by machining cracks of a given size and measuring the plate

compliance and crack opening displacement as a function of crack size. An "effective" stress intensity factor can be calculated from the applied force and the compliance of the specimen. Tests were performed at 10 Hertz, varying the stress intensity range and the value of the maximum stress intensity during cyclic fatigue, K_{max}. At fixed values of load and amplitude, the flaw propagation rate was constant within experimental sensitivity and the initial values of the parameters were used to correlate data. The mechanism of growth appeared to be the same as in graphite reinforced nylons, studied previously (17). That is, the stress concentration around the flaw tip causes the region around the tip to progressively decrease in strength, through fiber and fiber/resin interface failures. When the material is weakened locally to a critical point, crack propagation occurs rapidly and failure ensues. If the load is increased prior to catastrophic failure, the crack opens and grows to a new "equilibrium" size and the damage then occurs at a faster constant rate. In these glass reinforced PBT composites, the value of the crack propagation rate appears to be dependent on the stress history of the material.

IV. EXPERIMENTAL RESULTS AND CONCLUSIONS

Tensile Stress-Strain Behavior

Typical tensile stress-strain curves for two extremes of behavior are shown in Figure 1. Specimens from other populations have basically the same response. All populations exhibited a statistical variation of properties as illustrated in Figures 2 to 4. When plotted on Weibull coordinates, as illustrated in Figure 5 for population 2RH55, the ultimate properties appeared to conform to a bimodal Weibull function. The specimens in the low strength, low ductility tail of the distribution also appeared to exhibit a more brittle-type fatigue failure in subsequent fatigue tests. Also shown in Figure 5 is

a single example of a plot of $\ell n(-\ell n\ P)$ versus $\ell n\ t_B$ (fatigue life) for one set of fatigue testing conditions. In spite of the pronounced bimodal behavior of the ultimate properties, the fatigue life distributions conformed much more closely to a simple, two parameter Weibull function. Of the number of specimens used to define a given population (of the order of 20), usually 3 to 4 were in the low ductility, low strength tails of the ultimate property distributions, while no more than 1 or 2 would appear to form a short lifetime tail different than that of the remaining distribution. In either case it was almost impossible to define parameters to describe the low-probability tails with any reasonable degree of certainty. In order to estimate mean properties for the distributions, a two-parameter Weibull function was used to describe the longer, higher strength, higher ductility portion of the distribution (Table 2).

All stress-strain curves were non-linear to the point of failure. Within the experimental accuracy of the recording system, the response was approximately linear only to about 0.003 to 0.005 in/in tensile strain (i.e. the initial 10-20 percent of the stress-strain curve). An initial tangent modulus could be defined by the slope of this region. The results are indicated in Table 1.

The initial tangent modulus did not vary very much with treatment. There appears to be, at most, a 10 percent decrease in modulus with long-term exposure to water, accompanied by a greater degree of non-linearity of the stress-strain curve. This is likely associated with the change in ductility of the resin phase, but the presence of the fibers limits the change in stiffness of the material. The statistical variation of the order of $\pm$ 100,000 psi is also of the order of 10 percent and is likely associated with compositional variations from piece-to-piece and orientation differences from piece-to-piece associated with the molding process.

The theoretical modulus of a random-in-a-plane PBT composite containing 20 percent by volume of 6 mm fibers is of the order of 1,025,000 psi. Having

been injection molded, the specimens did have some orientation in the surface, which would lead one to believe that the calculation is conservative. Nevertheless, the experimental modulus is probably close to the theoretical value. A composite fiber efficiency of the order of 80 to 90 percent is consistent with good adhesion between phases. Proof of good adhesion independent of the effect of water treatment, will be presented in a later section using electron microscopic evidence.

The more interesting variables are summarized in Table 2. The first as-received population (1-RH55) is somewhat stronger and tougher than the second (2-RH55). The difference in strain-to-break is the most significant, the former having an average strain to break of 3.2 percent compared to 2.9 percent for the latter. The physical appearance of the 1-RH55 population was also much better. It was the only group of specimens without noticeable surface blemishes. Upon inquiry, it was discovered that the first batch was produced with a different mold than the others, which for some reason unknown to the manufacturer of the specimens resulted in a cleaner, more defect-free batch of specimens. It will be shown later that this condition of "improved" processing also resulted in a very significant increase in the average fatigue life of the population.

Since 300 of the specimens were of the type in population 2-RH55, this group should be considered the reference population. It should be noted, however, that the differences between 1-RH55 and 2-RH55 were washed out by long-term exposure to hot or boiling water. Once the ductility of the specimens deteriorated, all behaved in the same brittle manner.

Tensile strength, ductility (strain-to-break) and toughness (area under the stress-strain curve) all deteriorated upon exposure to hot or boiling water. As expected, the long-term effects were greater in boiling water,

than in hot water. Electron microscopic evidence indicated that neither the glass nor the interface was much affected by the treatment, but that the polymer phase was considerably more brittle. Thus, water absorption into the polymer phase was responsible for the deterioration of the composite properties. The average tensile strength was reduced by boiling water to 64 percent of that of the as-received material, while the strain-to-break decreased to 52 percent and toughness decreased to 28 percent of the values for the as-received material. The 70 degree water exposure caused corresponding deteriorations to levels of 81 percent, 69 percent and 47 percent respectively.

The exposure to 100 percent humidity at room temperature resulted in a small decrease in tensile strength (93 percent of as-received), but a substantial increase in strain-to-break (to 3.3 percent from 2.9 percent) and some increase in toughness (6 percent greater than as-received). In this case, the smaller amount of water absorption at lower temperature resulted only in a plasticization of the polymer phase, without the deterioration of the polymer that occurred because of the combined effects of high temperature and water absorption.

Fatigue Life

Fatigue tests have been carried out under cyclic tension at different maximum stress levels, keeping frequency and stress ratio R constant at 10 Hertz and 0.67 respectively. The testing conditions are summarized in Table 3.

Cumulative distribution functions for each population were calculated for the time-to-break, t_B, and are illustrated in Figures 6 and 7 for populations 2-RH55 and 4-BW192 respectively. When plotted on Weibull coordinates, in all cases the data conform to a straight line and can be described by a two-parameter Weibull function (except for the lowest one or two points as discussed previously and shown in Figure 5). Shape (α) and scale (t_o) factors as well as the average values of t_B and the coefficients of determination (r^2) are summarized in Table 4.

At the maximum fatigue stress levels used, none of the specimens survived one million cycles or more. It is clear from the data, however, that the hot and boiling water treated populations, being more brittle than the others, fail prematurely at the same relative stress level (i.e., relative to the average strength of the given population). In order to estimate an apparent endurance level for each population, several fatigue tests were run at lower stresses. The more ductile populations (2-RH55 and 3-RH100) appear to reach an endurance limit in the range of maximum stress of $L = \sigma_{max}/\langle\sigma\rangle = 0.65$ to 0.75, while the more brittle populations (4-BW192 and 5-HW504) required a reduction in maximum stress to of the order of L = 0.45 - 0.55. Thus, not only did the maximum allowable stress at the endurance limit decrease with a decrease in the average strength of the population, but a decrease in ductility appears to worsen the fatigue response, requiring a proportionally greater decrease in stress level to stay at the endurance limit of the material.

The effect of ductility on the fatigue response can be generalized by plotting elongation to break ε_b versus time-to-break t_B for equiprobability points in the respective distributions. All of the data are plotted in this manner in Figure 8. Within the accuracy of plotting the data in this manner, there appears to be a nearly linear relationship between the logarithm of ε_b and the logarithm of t_B at equiprobability points in the respective distributions, not withstanding the few points in the low-ductility tails that did not conform to simple Weibull statistics. The two numbers labeling each line in Figure 8 are an identification number for the population and the relative stress level, L, of the fatigue test (i.e., 1/0.90 signifies the first population listed in Tables 2 and 4, fatigue tested at a stress equal to 0.90 of the average strength of the population).

A single master plot of the data can be obtained by shifting along the absicca using a multiplicative factor of $L^2 = [\sigma_{max}/\langle\sigma\rangle]^2$. Although a well-defined single curve is not obtained, as shown in Figure 9, all data fall in a narrow band defined by two intersecting regions of space.

An implication of this exercise is that for a given value of elongation-to-break (i.e., ductility), there is a nearly constant value of the quantity $[\sigma_{max}/\langle\sigma\rangle]^2$ ℓn t_B, or $t_B \propto \exp - C/L^2$, where the constant C increases as a function of elongation-to-break. There is clearly a sharp change in response at $-$ ℓn ε_b = 3.45 - 3.55 (ε_b = 0.029 - 0.032), with the ductile materials exhibiting a much longer life at a given value of L than would be expected from an extrapolation of the data for the more brittle materials. For example, at a value of ε_b = 0.015, L^2 ℓn t_B = 3.6 to 3.8. If one defines an apparent endurance limit as $t_B = 10^5$ seconds (1 million cycles @ 10Hz), then L at the endurance limit is about 0.56 to 0.58. At a value of ε_b = 0.033, L^2 ℓn t_B = 5.7 to 6.3, and L at the endurance limit is about 0.70 to 0.74. From the average strength data of Table 1, the maximum fatigue stress at the endurance limits would correspond to roughly 6400 psi for an average specimen in the brittle population (e.g. population 4-BW192) and roughly 12,600 for an average specimen in one of the more ductile populations (e.g. population 2-RH55). The few fatigue tests run near or below the endurance limits confirm these estimates.

Cyclic Softening

The rate of strain was monitored during all cyclic fatigue tests. A typical curve of strain versus time, obtained in a load controlled fatigue test in which the load limits were held constant, is shown in Figure 10. Three different regions can be discerned during the softening process:

1) An initial, transition state, usually very short and always present, characterized by a macroscopic cyclic softening. In this stage, the

nonelastic strain increases rapidly under the constant peak stresses, until it reaches a steady rate of growth.

2) A region where a gradual softening occurs with a constant rate whose value depends on the sample characteristics and stress level. This state, resembling a steady-state creep of the material, comprises the greatest part of the fatigue process.

3) A final region where either the nonelastic strain increases rapidly until specimen failure occurs or the strain rate decreases to nearly zero so that no further change in the material is apparent. The latter occurs below the endurance limit of the material.

This continuous softening behavior is common in polymers with heterogenous microstructures, such as composite materials. The above-described softening process is not thermal in nature. The temperature of the material increased quickly to 5 to 20 degrees above the ambient temperature (depending on the stress level and amplitude) due to hysteretic self-heating and then remained constant upon reaching a steady state of heat transfer. The only transitions discernable in a differential scanning calorimeter commenced at about 225°C, so that the effect of a 20 degree rise in temperature on properties is negligible.

The total strain-to-break consisted primarily of the sum of the strains during the first two stages. The contributions during these two stages were estimated by extrapolating the "steady-creep" curve back to the origin of the plot to determine, ε_I, an initial strain due to a nearly instantaneous cyclic-softening. The strain contributed by the "steady-creep," ε_{II}, was calculated from the difference between the strain-to-break in fatigue ε_{bf} and the strain due to cyclic softing. In general, these two contributions were of the same order of magnitude, as illustrated by the data in Table 5. The magnitude of both contributions appear to depend on the stress level, increasing with in-

creasing maximum fatigue stress. For a given population under constant loading conditions, there was a complex distribution of values for ε_I and ε_{II}, the magnitude of which is characterized by the range of extreme values reported in Table 5. The sum of the two contributions, that is the total elongation-to-break in fatigue, was related to the elongation-to-break in the stress-strain tests. The trends in this regard are illustrated in Table 6. The data are divided into three groups: materials of high ductility (ε_b>3.3%), materials of intermediate ductility (3.1>ε_b>2.0%) and materials of low ductility (1.8>ε_b>1.3%). In general, the magnitude of the two contributions and the total strain-to-break in fatigue decrease with decreasing ductility. The ratio of elongation-to-break in fatigue to the elongation to break in a stress-strain test, $\varepsilon_{bf}/\varepsilon_b$, also tends to decrease with decreasing ductility. Thus, from Table 6 one can see that with the high ductility materials ε_{bf} attains 50 to 70% of the value of ε_b, while with the low ductility materials ε_{bf} can attain only 30 to 50 percent of ε_b.

This is still another indication that the embrittlement of the material causes a greater than proportional decrease in the fatigue properties.

During the second stage of deformation in fatigue, the rate of deformation during a specific test is nearly constant, (except very close to the endurance limit where it tends to decrease with time). A "steady-state" creep rate can be measured from the slope of the strain (at peak stress) versus time, as in Figure 10. In a series of tests on a given population under constant test conditions, the measured rate of deformation distributes as a normal distribution about a mean. A typical result as shown in Figure 11 for population 4-BW192 tested at different levels of maximum stress. The probability distribution curves are drawn using the variable $\ell n(d\varepsilon/dt)^{-1}$ with units of seconds per unit of strain. The low rate of deformation tail $P(\dot{\varepsilon}^{-1})_{\infty}$, represents long-lived specimens, analogous to the distribution

curves used to describe the distributions of time-to-break (Figure 7, for example). By analogy with the time-temperature superposition principles used to generate master curves of viscoelastic properties, the distribution curves were shifted along the time axis using a shift factor $a_{\dot{\varepsilon}^{-1}}$, where:

$$\ell n\ \dot{\varepsilon}_R^{-1} = \ell n\left(\frac{\dot{\varepsilon}^{-1}}{a_{\dot{\varepsilon}^{-1}}}\right) \tag{8}$$

That is to say, a given value of $\dot{\varepsilon}^{-1}$ is divided by the shift factor $a_{\dot{\varepsilon}^{-1}}$ in order to superimpose the resulting value on the reference curve. The embrittling effect of water treatment was examined by using all of the experimental data for populations 2-RH55 (the as-received state), 4-BW192 and 5-HW504 under all of the fatigue conditions studied. The resulting master curve is shown in Figure 12, using the as-received population at a maximum stress level L = 0.70 = $\sigma_{max}/\langle\sigma\rangle$ as the reference state. The appropriate shift factor could be divided into a scale factor dependent only on the level of the relative stress (L) and a shape factor that depended only on the water treatment:

$$a_{\dot{\varepsilon}}^{-1} = {}^{a}\text{scale} \cdot {}^{a}\text{shape} \tag{9}$$

where

$${}^{a}\text{scale} = f\ (\sigma_{max}/\langle\sigma\rangle) \tag{10}$$

and

$${}^{a}\text{shape} = 1.0 \text{ for the as-received state} \tag{11}$$

$${}^{a}\text{shape} = (\dot{\varepsilon}_R^{-1})/(\hat{\dot{\varepsilon}}_R^{-1}) \quad \text{for both water-treated populations} \tag{12}$$

where $\dot{\varepsilon}_R^{-1}$ is the inverse of the rate of deformation in the reference state at any point in the distribution and $\hat{\dot{\varepsilon}}_R^{-1}$ is the inverse of the rate of deformation in the reference state at the point in the distribution $P(\ell_R^{-1}) = 0.368$.

To a first approximation, the effects of peak stress and environment were separable. A changing relative stress state under constant environmental conditions caused a shifting of the distribution curve along the time axis, without changing the shapes of the distribution, while the environmental treatment caused a change in the shape of the distribution curve.

The appropriate scale factor is shown in Figure 13, plotted on the semi-logarithmic coordinates of $\ln a_{scale}$ versus $0.7\ (\sigma_{max}/\langle\sigma\rangle)^{-1}$. The scale factor is thus 1.0 at the reference stress state of $\sigma_{max}/\langle\sigma\rangle = 0.7$ and varies very nearly linearly in semi-logarithmic coordinates, as might be expected. All the data except for one run, namely population 4-BW192 tested at L = 0.65, fell quite well on a single master curve. The reason for the deviation of those data is not clear.

The reference state is arbitrary. If one chose the water-boiled population 4-BW192 at L = 0.70 as the reference state, the result would be described by Figure 14. The same scale factor is used, but the shape factors are inverted ($a_{shape} = 1.0$ for 4-BW192).

Figure 15 illustrates the difference in shape between the as-received and the water-treated populations when compared at the same level of relative maximum stress in fatigue L = 0.7. If one considers the as-received state as the reference state, the data for the water-treated populations are shifted by the appropriate scale factor a_{scale}. When shifted to equivalent levels of stress, however, the shapes of the two distributions are quite different. The water-treated populations have a much broader distribution. Thus, the embrittlement of the material results in a lowering of strength and a broadening of the fatigue response. This means that at the same level of relative maximum stress in fatigue, one would encounter a larger number of premature failures even though the average response (in this case at P = 0.368) of the two

populations is the same. The shape of the cumulative distribution and thus the reliability of the material is affected by the environmental conditioning.

Effect of Test Frequency on the Rate of Deformation During Fatigue

Specimens from population 2-RH55 were tested under cyclic tension between the frequencies of 1 to 35 Hertz, at a number of maximum stress levels and at a constant stress ratio R equal to 2/3. The rate of strain at peak stress was monitored continuously as a function of frequency, and the frequency range was scanned several times for each specimen.

Figure 16 illustrates the behavior of all specimens. Upon scanning the frequency for the first time from 1 to 35 Hz the deformation rate decreased rapidly until a minimum was reached at 20 Hz and then it increased. Upon re-scanning the range 35 to 1 Hz., the rate of deformation dropped continuously, not reproducing the rates from the original scan. The third scan, 1 to 35 Hz, resulted in a steady increase in rate of deformation, again not reproducing the first or second scans. It was only after the fifth scan that the data could be reproduced on successive passes. The "steady state" rate of deformation then appeared to increase linearly with frequency, with the slope dependent on the maximum applied stress. Beyond a maximum applied stress level of $L = 0.75$, the response was time dependent during the whole life of the specimen. The temperature increased no more than 10-20 degrees centigrade over the frequency range, not enough to account for the large excursions of behavior.

Thus it is clear that the viscoelastic properties of the material under fatigue conditions are changing continuously with time. In the region near the endurance limit, an initial transient behavior is followed by an apparently "steady-state" response. At stresses above the endurance limit, the viscoelastic properties appear to change almost continuously with time.

Effect of Stress Ratio (Amplitude) on the Rate of Deformation During Fatigue

Specimens from population 2-RH55 were tested under different amplitudes of loading at a fixed frequency of 10 Hertz and at two different maximum stress levels of L = 0.6 and 0.7. The test conditions are summarized in Table 7. The stress ratio R was scanned over the range 0.42 to 0.92 several times until a "steady state" deformation rate was attained. A typical result is illustrated in Figure 17. Once again, the deformation rate decreased continuously through several scans, until a steady-state was attained from the fourth scan on.

The rate of deformation response in "steady-state" is quite complex, showing a minimum in the range of R = 0.55 to 0.65. The value of R at the minimum increases slightly with the maximum stress level L. The magnitude of the rate of deformation also increases with (L) and above a value of L = 0.70 the specimen fails while the material is still in a transient state.

At higher amplitudes (low values of R) there is considerable hysteretic heating that causes the material to ultimately fail in thermal fatigue. On the contrary, virtually no hysteretic heating is apparent at smaller amplitudes (values of R greater than 0.6) and the fatigue failure is characterized by a crack propagation mechanism. Under all conditions, there is an apparent creep occurring that becomes more important as the maximum applied stress increases.

Thus, both the amplitude and the maximum applied stress have a strong effect on the fatigue failure mechanism. Under small amplitudes and high peak stresses, that is to say quasi-static loading conditions, an apparent creep becomes the predominant deformation mechanism. Under large amplitudes and high peak stresses, hysteretic heating leads to a thermal fatigue mechanism. At lower peak stresses and small or intermediate levels of amplitude, the fatigue failure is more typical of a crack propagation controlled failure mechanism.

It appears that all three mechanisms of failure contribute to the response over the range of frequency, maximum stress and stress amplitude normally encountered in the testing of composite materials. Furthermore, under these circumstances, the observed failure mechanism is likely to be sensitive to both the geometry of the test piece and the type of fatigue test used, thus making it very difficult to correlate laboratory tests with field tests on particular types of hardware.

Electron Microscopy Studies of the Fracture Surfaces of Tensile Tested and Fatigued Specimens.

Scanning electron micrographs of the fracture surfaces of randomly chosen specimens from each population, tested in both fatigue and under a ramp loading of 0.2 inches/minute (stress-strain tests), were examined. Figures 18 to 22 are illustrative of the results of these studies.

One common feature of all the photographs taken is that the fiber pullout length does not change very much because of either exposure to water, the level of the stress or the type of test. From the length of the fibers pulled out of the surface parallel to the loading axis, it is possible to estimate the strength of the interfaces using a shear lag analysis. From the Kelly-Tyson shear-lag model, the yield strength of the "interface," or the resin at the interface, is;

$$\tau = \frac{\sigma d_f}{2\ell_c} \tag{13}$$

where σ is the average fiber strength, d_f is the average fiber diameter and ℓc is the critical length of the fibers (taken here to be two times the maximum pullout length of fibers oriented parallel to the loading axis). Using an average fiber strength of 250,000 psi, an average fiber diameter of 4×10^{-4} in. and the measured values of critical length, one calculates an average interface strength τ of the order of 3,500 to 6,000 psi. The variation

from point-to-point on a given specimen is greater than the differences from specimen to specimen. This bond strength is about the same as the yield strength of the PBT matrix. Thus it is felt that the adhesion between phases is relatively high and not strongly affected by the exposure to humidity, hot water or boiling water. It is likely that neither the fiber strength nor the interfacial strength were much affected over the range of environmental conditions studied, but rather that the major differences in behavior are attributable to the change in ductility of the PBT phase.

Figures 18 and 19 illustrate fracture surfaces for the as-received population 2-RH55 under ramp loading and fatigue respectively. Although there seems to be a difference in the appearance of the surfaces under the two types of loading, the distinction is misleading. Figure 19 shows two details from exactly the same fracture surface, but at two different points. Near the far edge of the specimen the fracture appears to have occurred with less plastic deformation than in the center of the fracture plane. In fact, the variation in appearance on a given fracture plane is considerably larger than the differences from specimen to specimen.

Without a preknowledge of what one was looking at, it would be very difficult to distinguish the fractures generated by ramp loading from those generated by fatigue. We could not find characteristic rings or other fatigue markings to distinguish one type of failure from the other.

Examination of population 3-RH100, exposed to high humidity, indicated a much higher degree of resin deformation on the fracture surface, as illustrated by Figure 20. Among the specimens examined, one could find relatively few areas of low resin ductility.

Figures 21 and 22 illustrate fracture surfaces of specimens exposed to boiling water (population 4-BW192). The resin appeared to fracture in a more

brittle fashion and in many places appeared to be very powdery. The interfaces at pulled out fibers were much sharper than before, even though the pull-out lengths were roughly the same.

It appears that the differences in mechanical response, in both ramp and fatigue loading, are attributable primarily to the ductility of the resin phase. Water absorption due to high humidity at ambient temperature plasticizes the resin phase, while exposure to hot and boiling water embrittles the resin phase, probably through degradation.

Crack Propagation Rates

Crack propagation tests were made using compact tensile specimens. The two conditions studied were materials in the as-received state and after 192 hours in boiling water. Crack propagation was studied as a function of both maximum applied stress and stress amplitude, at a fixed frequency of 10 Hz.

Continuous monitoring of the upper limit of stroke at the point of load application was obtained by feeding the stroke output signal into a sampling and hold device. From the ratio of the upper limit of the stroke to the peak load, one can obtain an instantaneous compliance for the notched plate:

$$C = \frac{u_{max}}{P_{max}} \tag{14}$$

The change in compliance with time was monitored and an "effective" crack propagation rate was defined as:

$$\frac{da}{dt} = \left(\frac{dC}{dt}\right) / \left(dC/da\right) \tag{15}$$

The derivative dC/da was calculated from a calibration run in which compliance was measured as a function crack size in a prenotched specimen.

An "effective" plane stress intensity factor was also computed from:

$$K^2 = \frac{EP^2}{2W(1-\nu^2)} \left(\frac{dC}{da}\right) \tag{16}$$

where E is the elastic modulus, W is the width of the plate, ν is Poisson's ratio, P is the load and $(^{dC}/da)$ is the first derivative of the compliance with respect to the crack length. Maximum and minimum values of K could be calculated from the maximum and minimum values of the applied load during fatigue.

Effective propagation rates were then correlated as a function of the stress intensity factors using the Erdogan Equation:

$$\frac{da}{dt} = \beta K_{max}^{\alpha 1} \Delta K^{\alpha 2} \tag{17}$$

$$= \beta K_{max}^{m} (1-R)^{\eta} \tag{18}$$

where β, m and η are constants, K_{max} is the maximum applied stress intensity factor during fatigue and R is the ratio of minimum to maximum stress intensity, $R = K_{min}/K_{max}$.

A critical value of the stress intensity factor, Kc, was also measured by the standard technique (44).

Results for the two environmental conditions are given below:

<u>As-Received</u> $Kc = 11{,}100 \pm 600$ $^{lb}f/in^{3/2}$

For $5000 < K_{max} < 10{,}000$ $^{lb}f/in^{3/2}$

$1/3 < R < 2/3$

frequency = 10 Hz

	$\frac{da}{dt}\frac{inches}{min.}$ @ R = 2/3	
	K_{max} = 5,000	10,000
$\frac{da}{dt}\frac{inches}{min.} = 3.4 \times 10^{-12} K_{max}^{2.6} (1-R)^{2.3}$	1.13×10^{-3}	6.8×10^{-3}
1st pass $r^2 = 0.90$		

$\frac{da}{dt}\frac{\text{inches}}{\text{min.}} = 1.3 \times 10^{-11} K_{max}^{2.4} (1-R)^{2.3}$		0.78×10^{-3}	4.1×10^{-3}
2nd pass	$r^2 = 0.85$		
$\frac{da}{dt}\frac{\text{inches}}{\text{min.}} = 2.0 \times 10^{-11} K_{max}^{2.3} (1-R)^{2.3}$		0.51×10^{-3}	2.5×10^{-3}
3rd pass	$r^2 = 0.91$		

After 192 hours in Boiling Water

$K_c = 7,000 \pm 500$ $^{lb}f/in^{3/2}$

For $3,000 < K_{max} < 6,000$ $^{lb}f/in^{2/3}$

$1/3 < R < 2/3$

frequency = 10 Hz

		$\frac{da}{dt}\frac{\text{inches}}{\text{min.}}$ @ R = 2/3	
		K_{max} = 3500	6000
$\frac{da}{dt}\frac{\text{inches}}{\text{min.}} = 1.9 \times 10^{-23} K_{max}^{6.1} (1-R)^{4.1}$		8.7×10^{-4}	2.3×10^{-2}
1st pass	$r^2 = 0.96$		
$\frac{da}{dt}\frac{\text{inches}}{\text{min}} = 1.2 \times 10^{-22} K_{max}^{5.8} (1-R)^{3.6}$		8.3×10^{-4}	1.9×10^{-2}
2nd pass	$r^2 = 0.89$		

First of all, the results appear to be dependent on the stress history imposed on the material. After making an initial set of measurements, the conditions of maximum stress and amplitude were repeated and new values of da/dt were calculated. For the as-received material, the rate of propagation continued to decrease with time and appeared to be less sensitive to the applied stress.

The propagation rates measured here are not useful for estimating the fatigue life of the tensile specimens used previously, since the effects of creep, so apparent in the prior tests, do not seem to be as important in the crack propagation tests, where the magnitude of the load is much less.

The effect of the boiling water was to lower the critical stress intensity factor, and to make the crack propagation rate much more sensitive to the stress intensity factor, as would be expected for a weaker and more brittle material. The stress-history dependence of the water-treated materials was not as marked as with the as-received materials. After the second pass the results seemed to stabilize and become much less dependent on stress history.

The mechanism of damage propagation appeared to be the same as in the graphite reinforced nylons studied previously (17), but the highly ductile nature of the glass reinforced PBT composites introduced a time and stress history dependence and a creep effect in the unnotched material that complicated the fatigue response, manyfold. A much more sophisticated approach will be required to utilize fracture mechanics data to evaluate the fatigue behavior of these materials.

ACKNOWLEDGEMENT

This research is sponsored by The Army Materials and Mechanics Research Center, Watertown, Massachusette, with Dr. M. Roylance as Technical Supervisor.

BIBLIOGRAPHY

1. Modern Plastics, Encyclopedia, 61 (1977-1978).
2. Kase, S., J. Polym. Sci., 11, 425 (1953).
3. Fedors, R.F., J. Appl. Polym. Sci., 19, 787 (1975).
4. Valanis K.C. and U Yilmazer, J. Polym. Sci., Phys. Ed., Vol. 16, 555 (1978).
5. Valanis K.C. and U Yilmazer, J. Polym. Sci., Polym. Phys. Ed., Vol. 15, 1101 (1977).
6. Zhurkov, S.N., V.A. Kuksenko and A.I. Slutsker, Sov. Phys. - Solid State, 11(2), 238 (1969).
7. Epstein, B., J. Appl. Phys. 19, 140 (1948).
8. Weibull, W., J. Appl. Mech., 18, 293 (1951).
9. Bury, K.V., Statistical Models in Applied Science, J. Wiley & Sons, N.Y. (1975).
10. Rosen, B.W., C. H. Zweben, MASA Contractor Report NASA-CR-2057, August (1972).
11. Halpin, J.C., J.R. Hopf, W. Goldberg, J. Comp. Mat. 4, 462 (1970).
12. Halpin, J.C., J. Comp. Mat. 6, 208 (1972).
13. Di Benedetto, A.T., G. Salee, R. Hlavacek, Poly. Eng. Sci., 15 (4), 242 (1975).
14. Hahn, H.T., R. Y. Kim. J. Comp. Mat. 9, 297 (1975).
15. Knight, M., H.T. Hahn, J. Comp. Mat. 9, 77 (1975).
16. DiBenedetto, A.T., Salee, G., Poly Eng. Sci. 18 (8), 634-42 (1978).
17. DiBenedetto, A.T., Salee, G., Poly Eng. Sci. 19, 7, 512, (1979).
18. Freudenthal, A.M., E.J. Gumbel, Trans. Roy. Soc. Lond. Ser. A216, 309 (1953).
19. Beardmore P. and S. Rabinowitz, Appl. Polym. Symp., No. 24, 25 (1974).
20. Dharan, C.K.H., J. Mat. Sci., 10, 1665 (1975).
21. Williams, J.C., J. Mat. Sci., 12, 2525 (1977).

22. Mills, N.J. and N. Walker, Polymer, Vol. 17, 335 (1976).

23. Skibo, M.D., R.W. Hertzberg, J.A. Manson and S.L. Kim, J. Mat. Sci., 12, 531 (1977).

24. Radon, J.C., J. Macromol. Sci., Phys., B14(4), 511 (1977).

25. Kambour, R.P., J. Polym. Sci., Macromol. Rev., Vol. 7, 1 (1973).

26. Martin, G.C. and W.W. Gerberisch, J. Mat. Sci., 11, 231 (1976).

27. Manson, J.A. and R.W. Hertzberg, Cri. Rev. in Macro. Sci., 1, 433 (1973).

28. Manson, J.A., R.W. Hertzberg, "Fatigue Failure in Polymers," Crit. Rev. Macromole. Sci. 1, 433 (1973).

29. Ferry, J.D., "Viscoelastic Properties of Polymers," Wiley, New York 1961.

30. Bouda, V., V. Zilvar and A.J. Staverman, J. Polym. Sci., Polym. Phys. Ed., Vol. 14, 2313 (1976).

31. Crawford, R.J., and P.P. Benham, Polymer, Vol. 16, 908 (1975).

32. Paris, P.C., and F. Erdogan, Trans. ASME, Ser. D., 85-4, 528 (1963).

33. Radon, J.C. and L.E. Culver, Polym. Eng. Sci., Vol. 15(7), 500 (1975).

34. Radon, J.C., and L. E. Culver, Polym. Eng. Sci., Vol. 15(7), 507 (1975).

35. Sauer, J.A., A.D. McMaster and D.R. Morrow, J. Macromol. Sci., Phys., B12(4), 535 (1976).

36. Radon, J.C. and L.E. Culver, Polymer, Vol. 16, 539 (1975).

37. Mukherjee, B., and D.J. Burns, ASTM STP, 511, 43 (1972).

38. Hertzberg, R.W., J.A. Manson, and W.C. Su, ASTM STP, 536, (1973).

39. Ishai, Ori, Polym. Eng. Sci., Vol. 15(7), 486 (1975).

40. Ishai, Ori, Polym. Eng. Sci., Vol. 15(7) 491 (1975).

41. Bott, T.R., and A.J. Barker, Trans. Instr. Chem. Engrs, 47, T188 (1969).

42. Browning, C.E., 28th, Ann. Tech. Conf., SPI Reinforced Plastics/Composites Institute, Sect. ISA (1973).

43. Mai, Y.W., Eng. Sci., Vol. 16(6) 400 (1976).

44. ASTM Standard Method E-399-74.

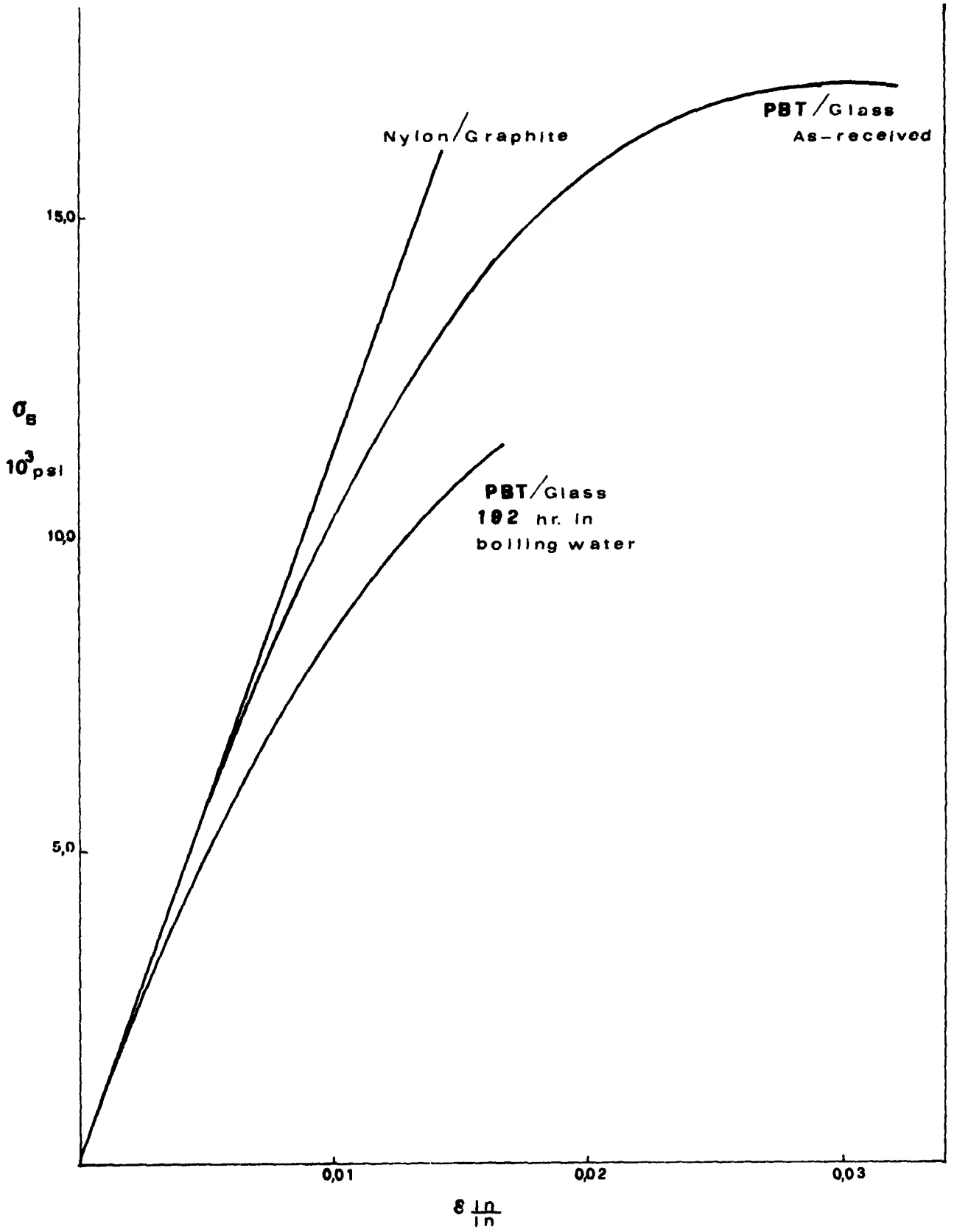

FIG. 1 Stress-Strain Curves for Glass Fiber Reinforced PBT Composites
(Cf. Graphite Reinforced Nylon AMMRC-CRT77-12)

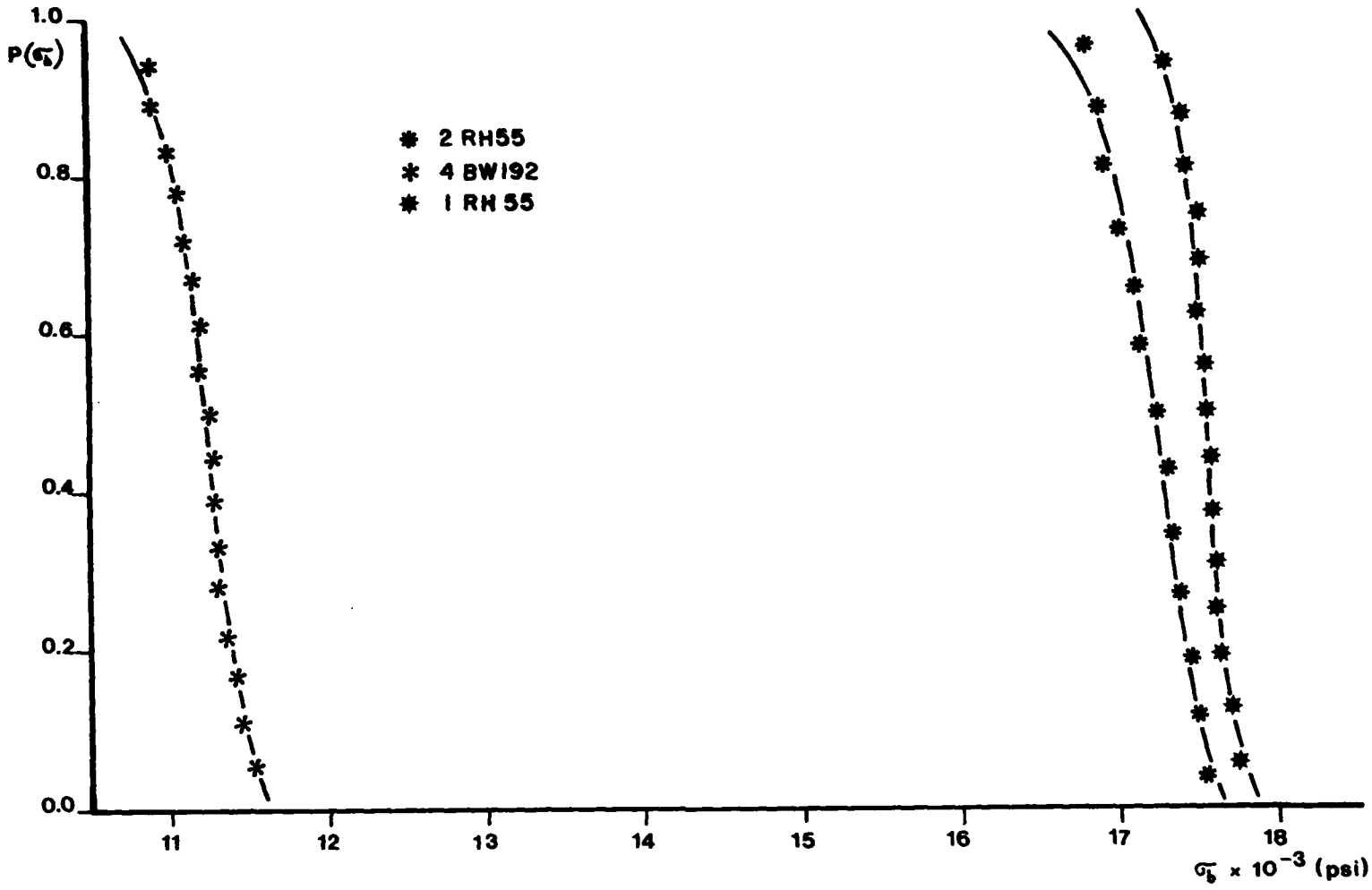

FIG. 2 Distributions of breaking stresses

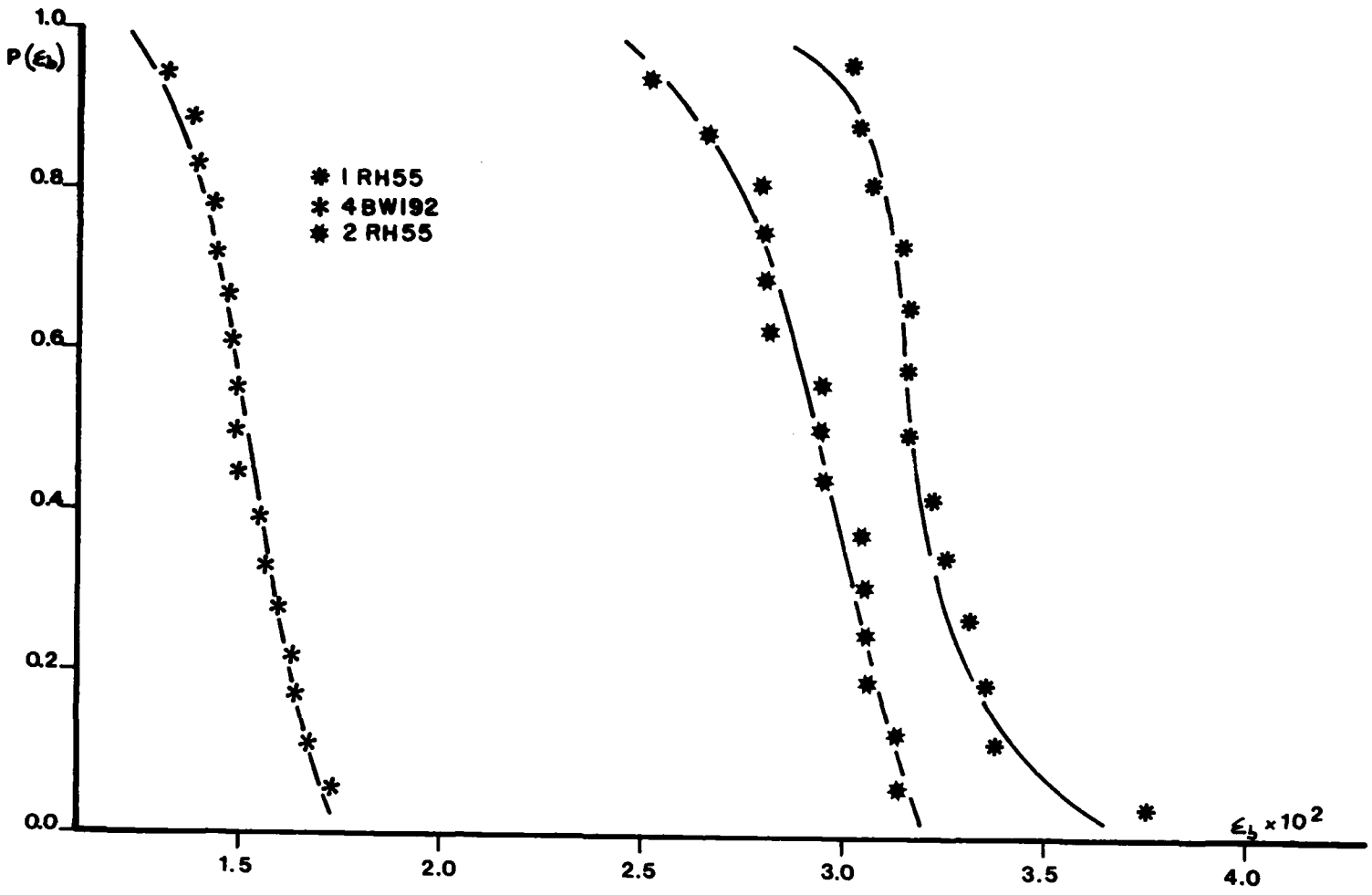

FIG. 3 Distributions of breaking strains

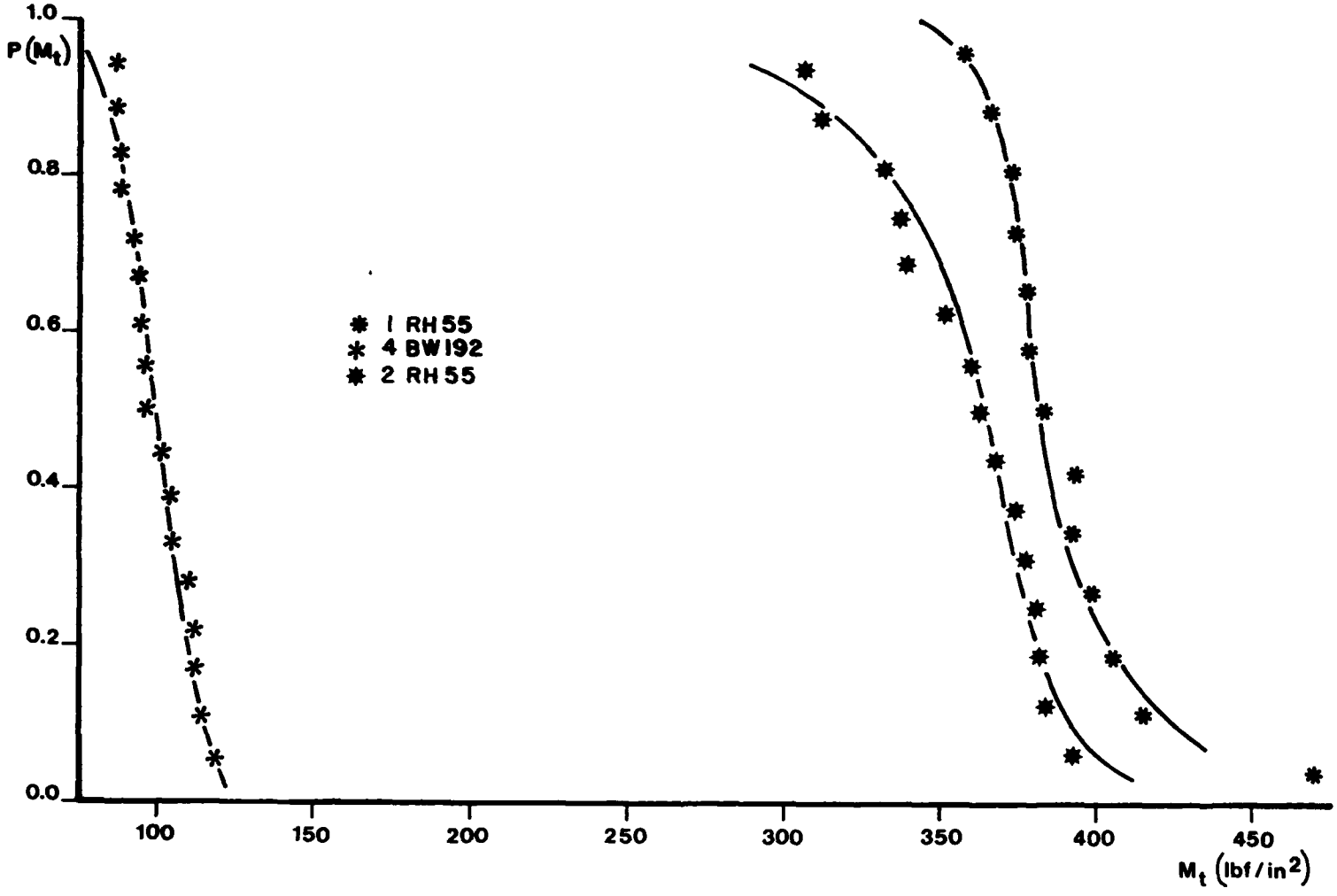

FIG. 4 Distributions of toughnesses

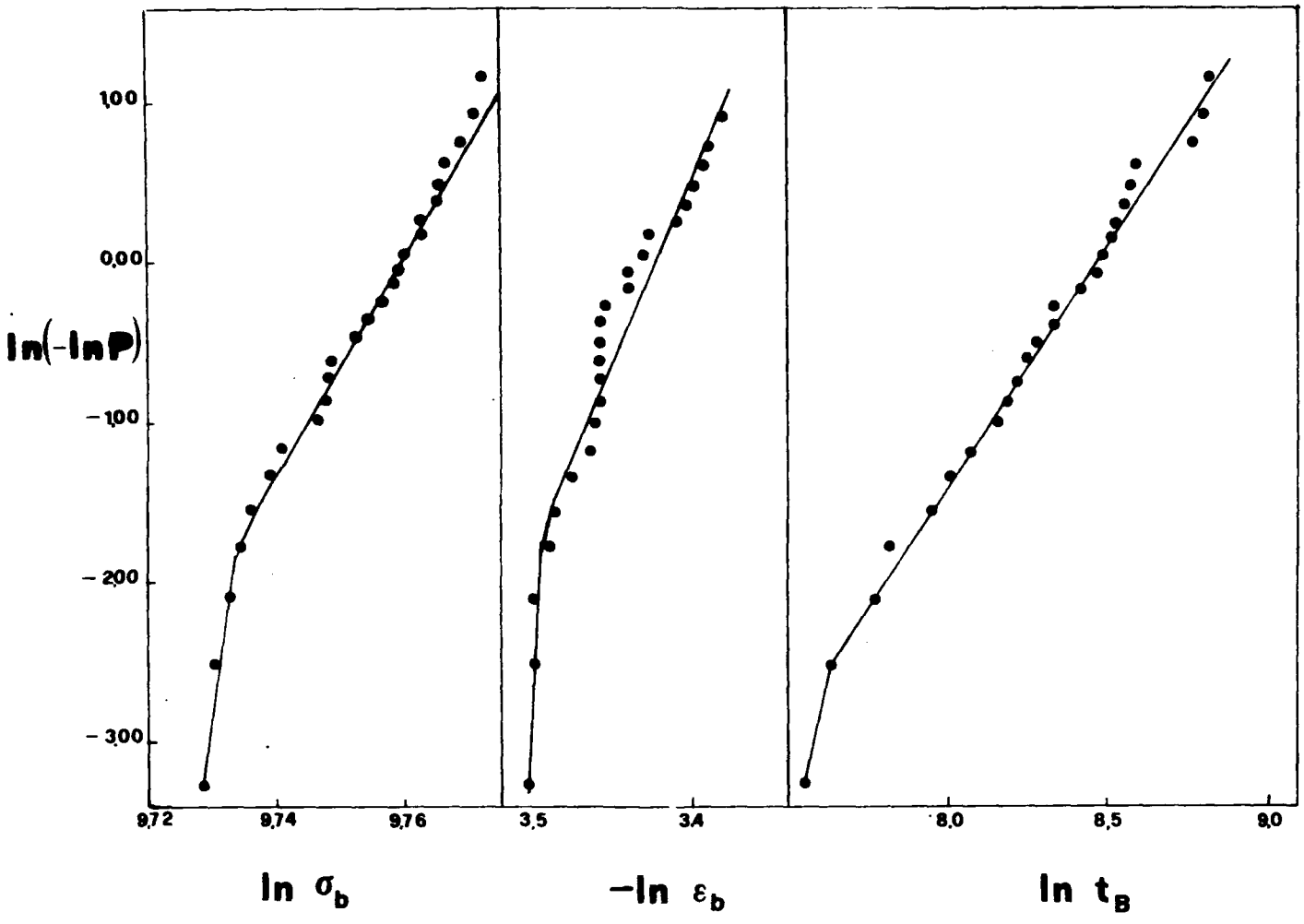

FIG. 5 Typical Weilbull Plots of Strength, Elongation-To-Break and Time-To-Break for Population 2-RH55

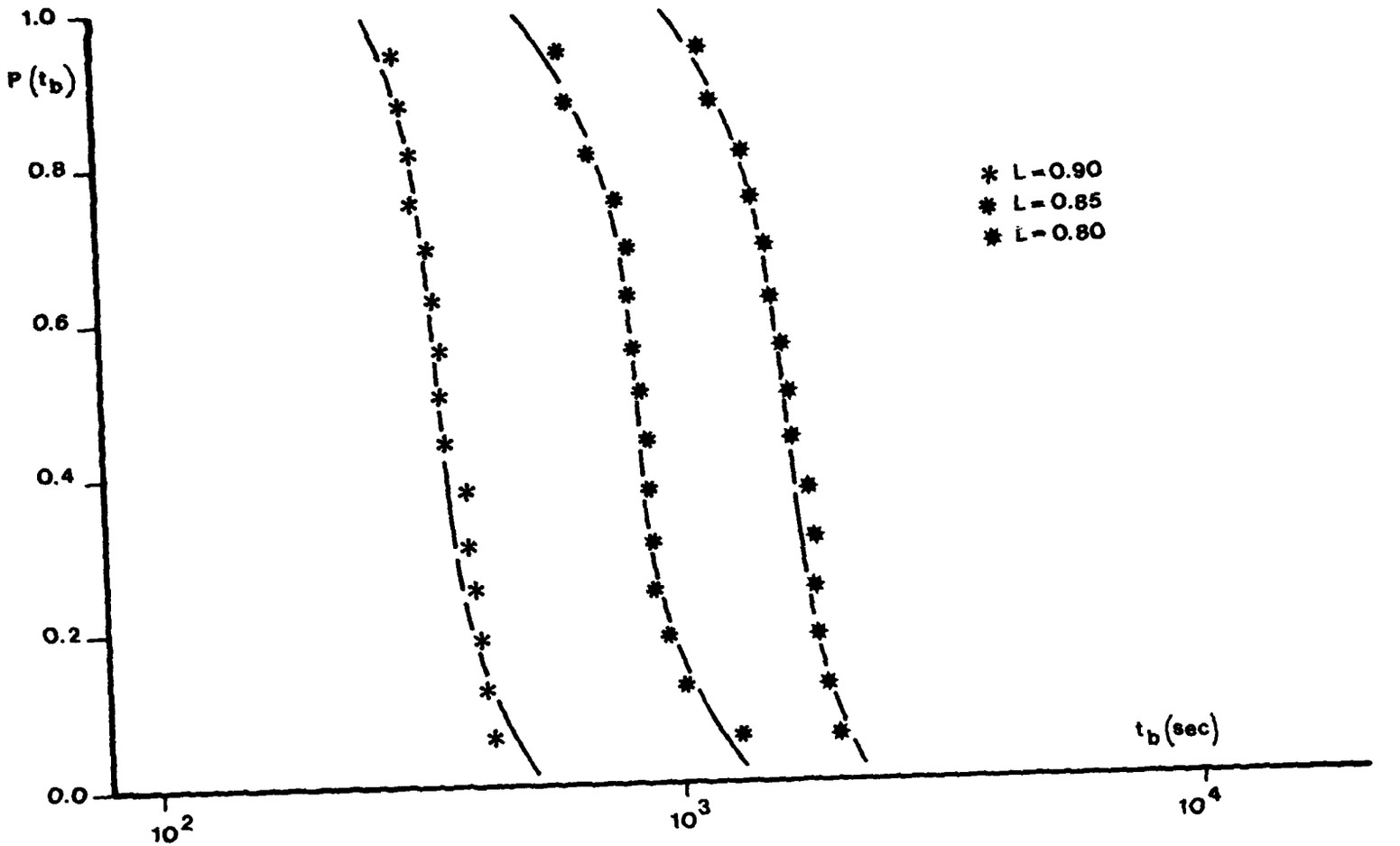

FIG.6 Distributions of lifetimes for 2-55RH

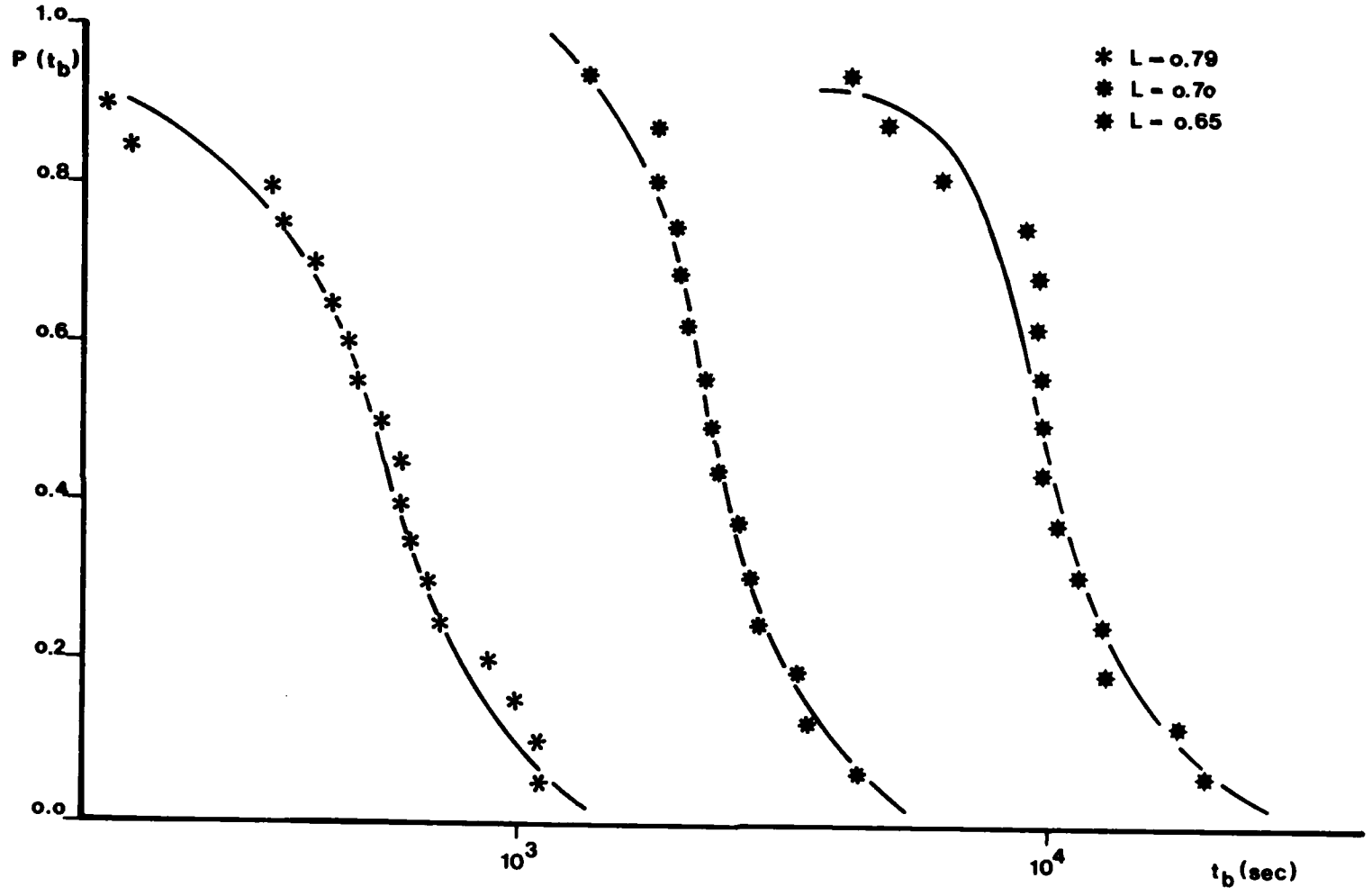

FIG. 7 Distributions of lifetimes for 4 - BW 192

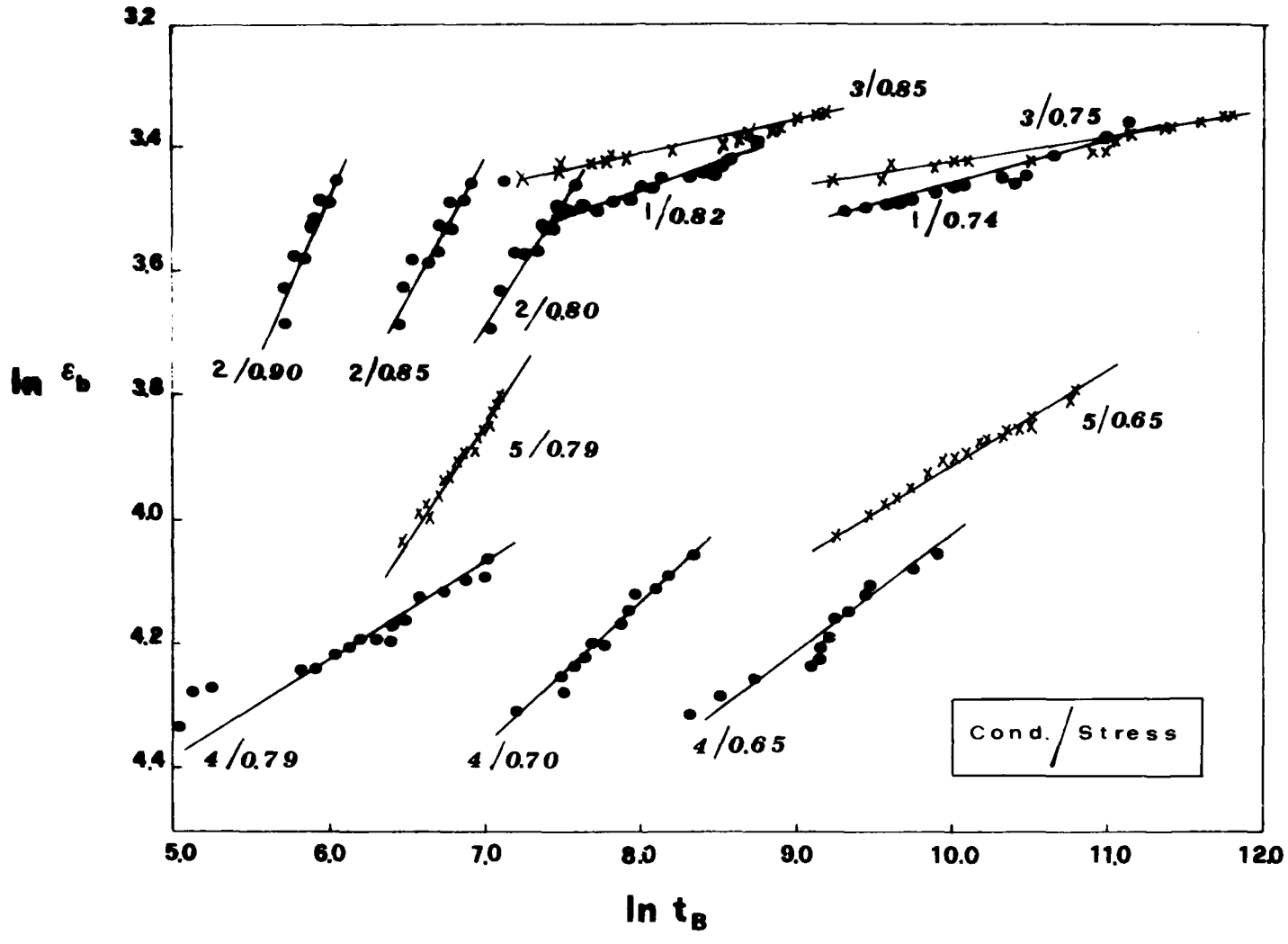

FIG. 8 Cross Plot of Elongation-to-Break versus Time-to-Break at Equiprobability Points of the Distributions

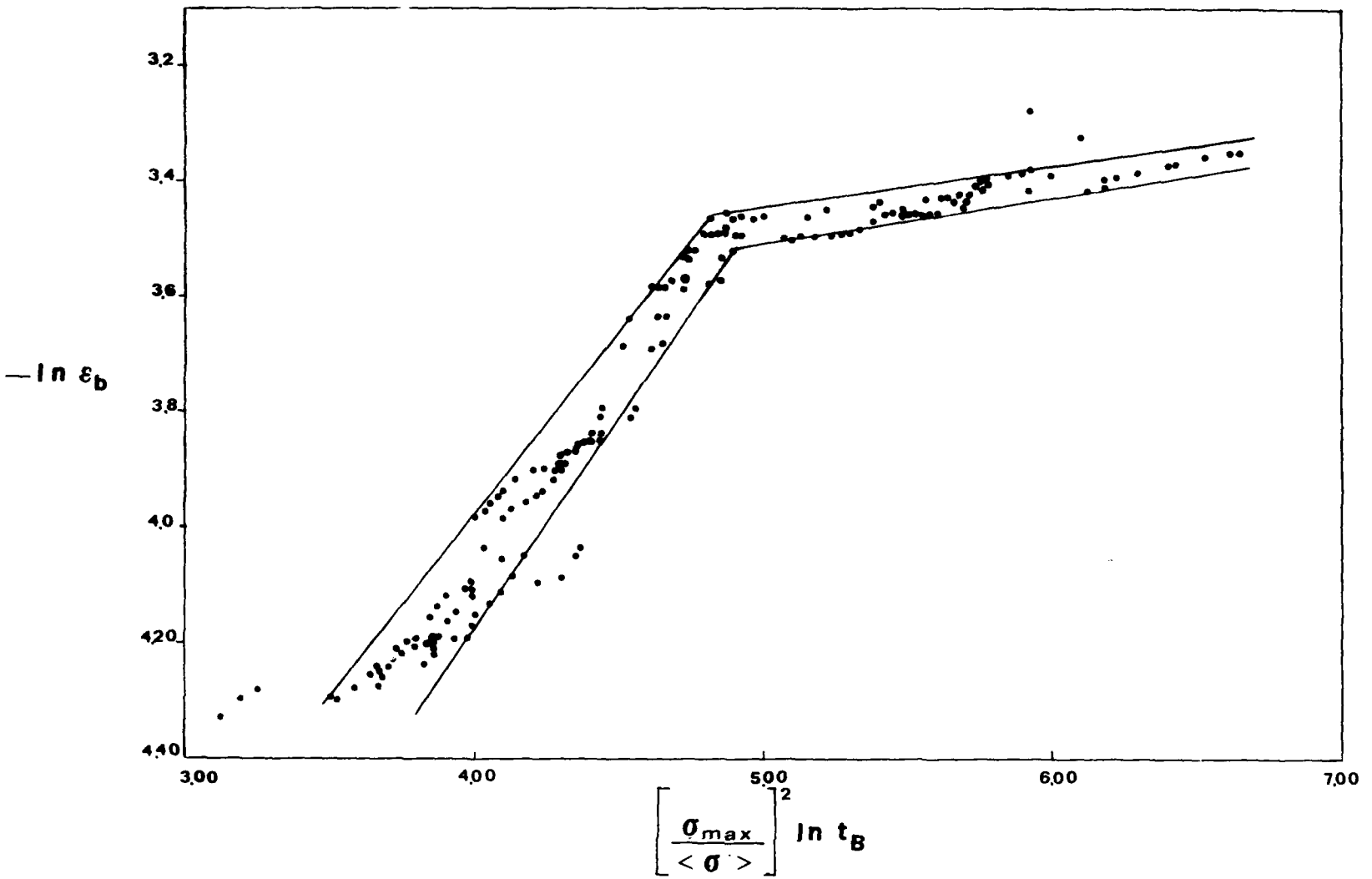

FIG. 9 Master Plot of Elongation-to-Break versus Time-to-Break

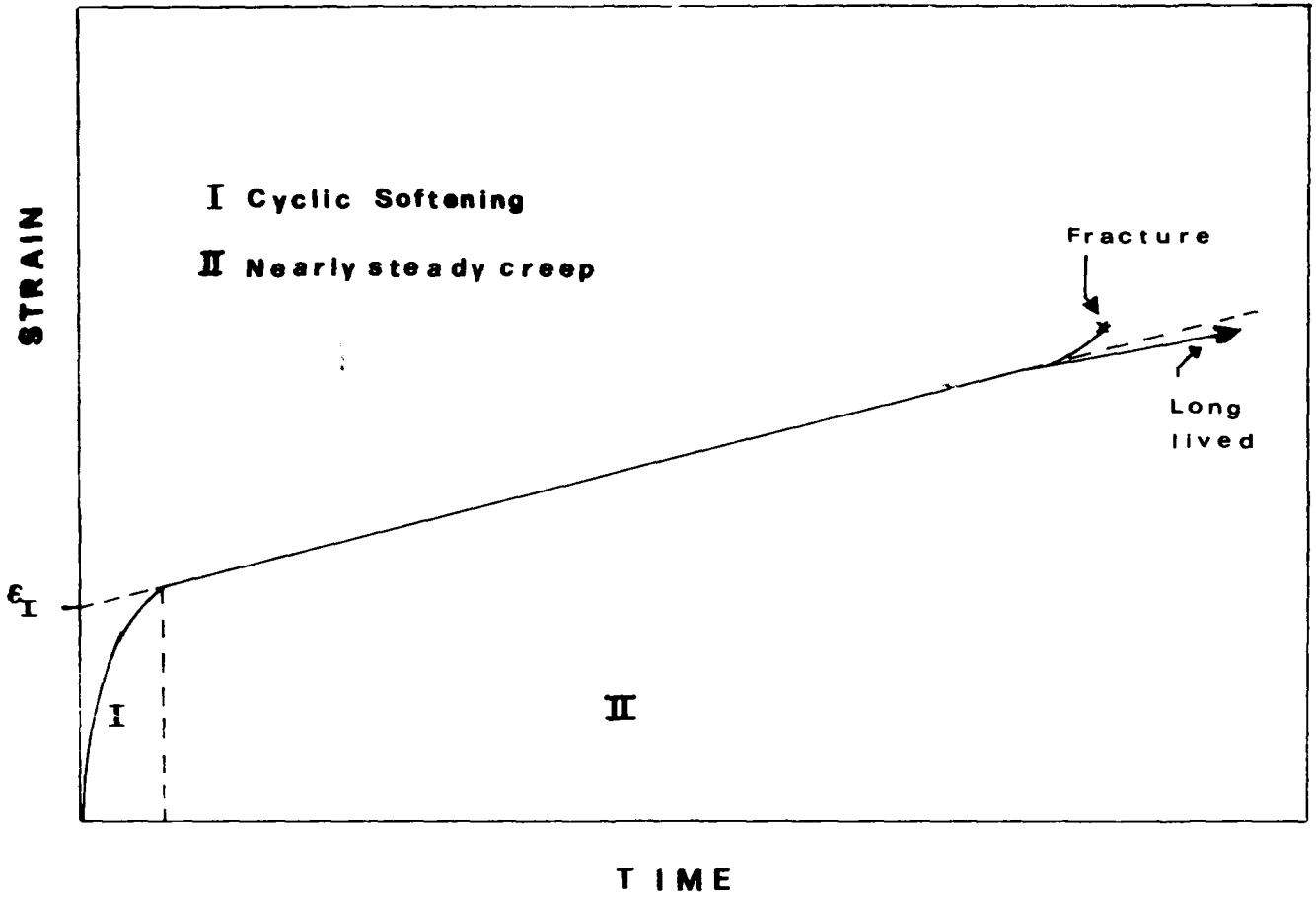

FIG. 10 Typical Fatigue Strain Curve for Glass Fiber Reinforced PBT Composite (Peak strain versus time in Fatigue test)

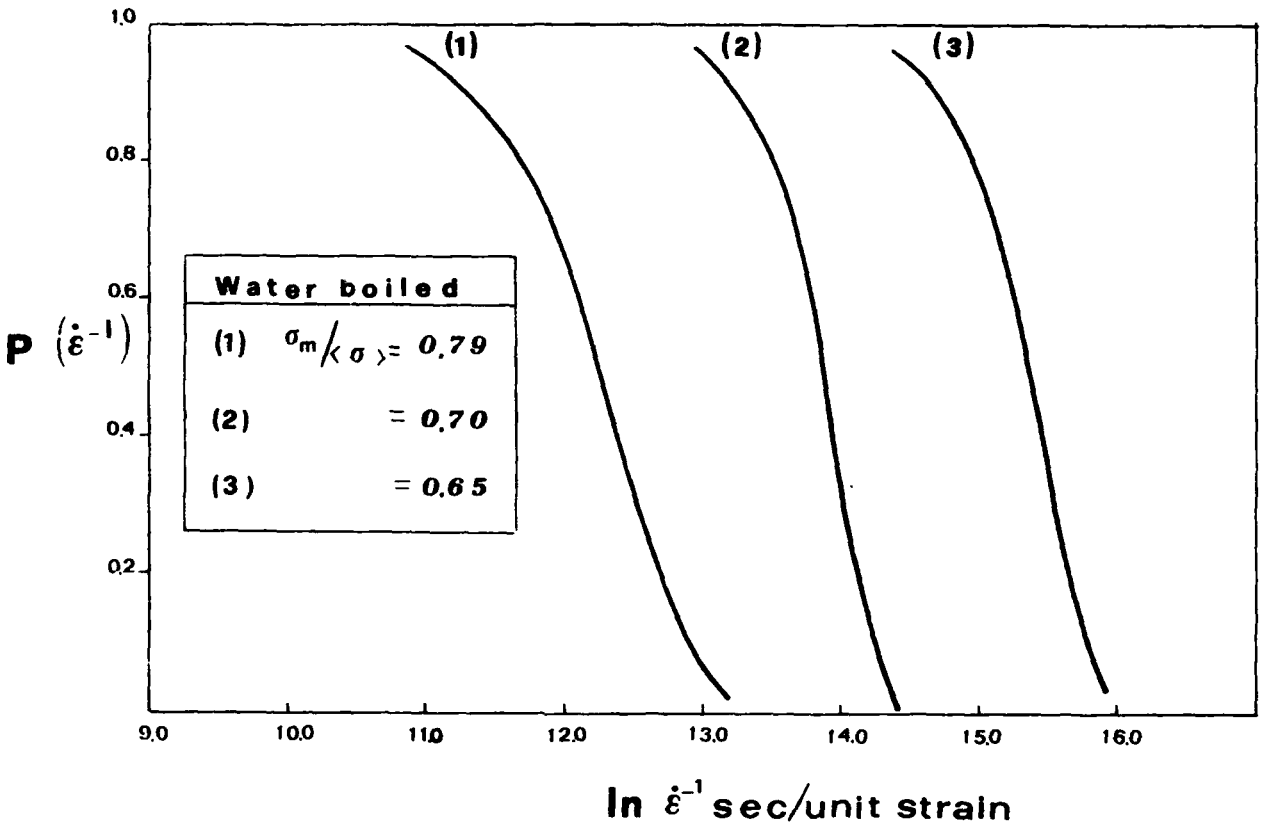

FIG. 11 Probability Distributions for the Inverse of the Rate of Strain During Fatigue for Population 4-BW192

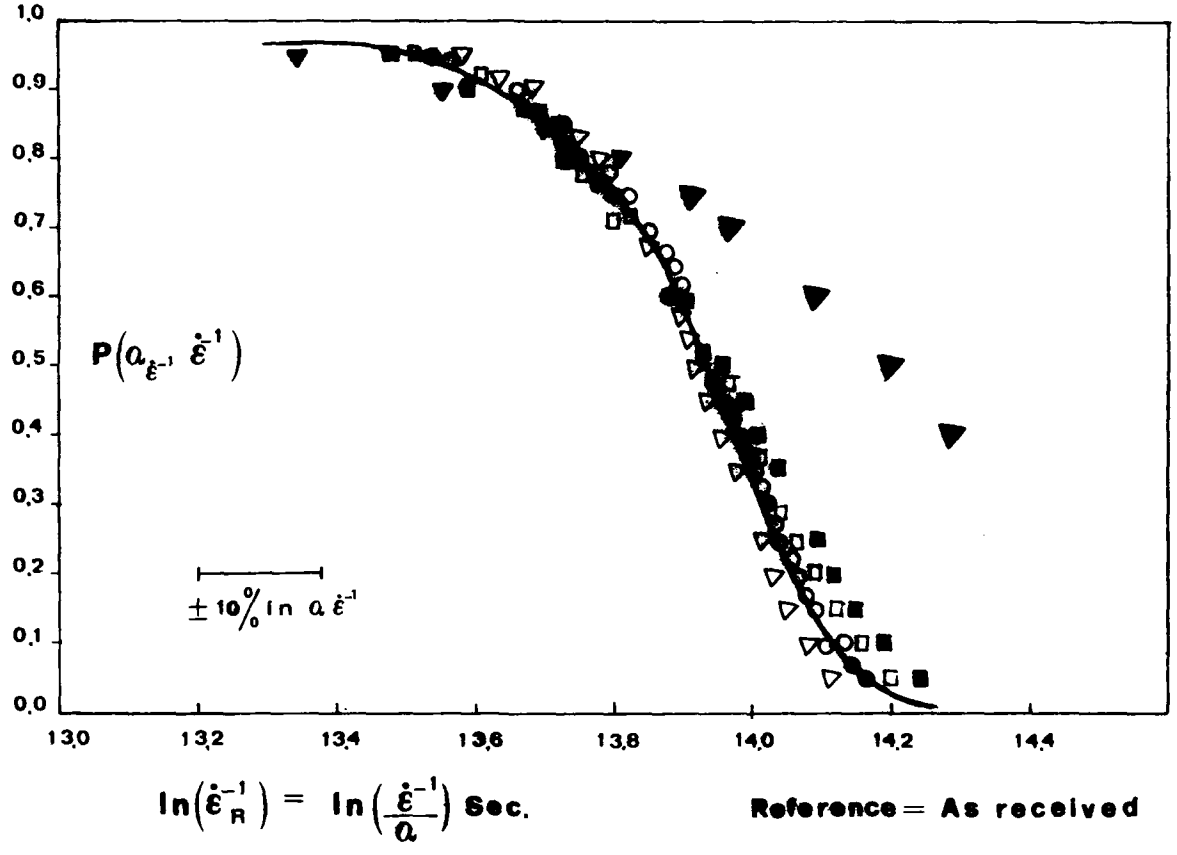

FIG. 12 Master curve for the Distribution of the Inverse of the Rate of Strain During Fatigue of Water Exposed Composites (Population 2-RH55 at L = 0.7 used as Reference State)

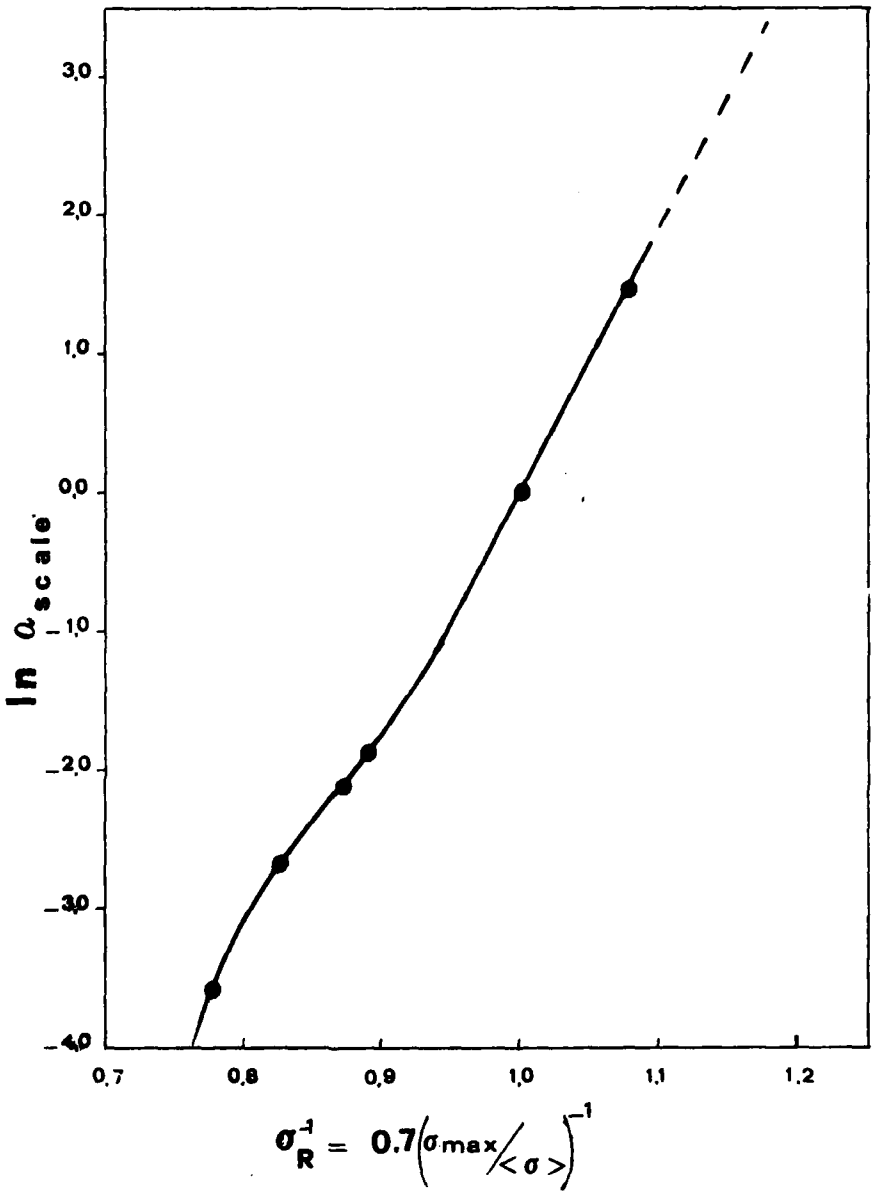

FIG. 13 Scale Shift Factor as a Function of Reduced Stress
(For use with Master Curve Figure 12)

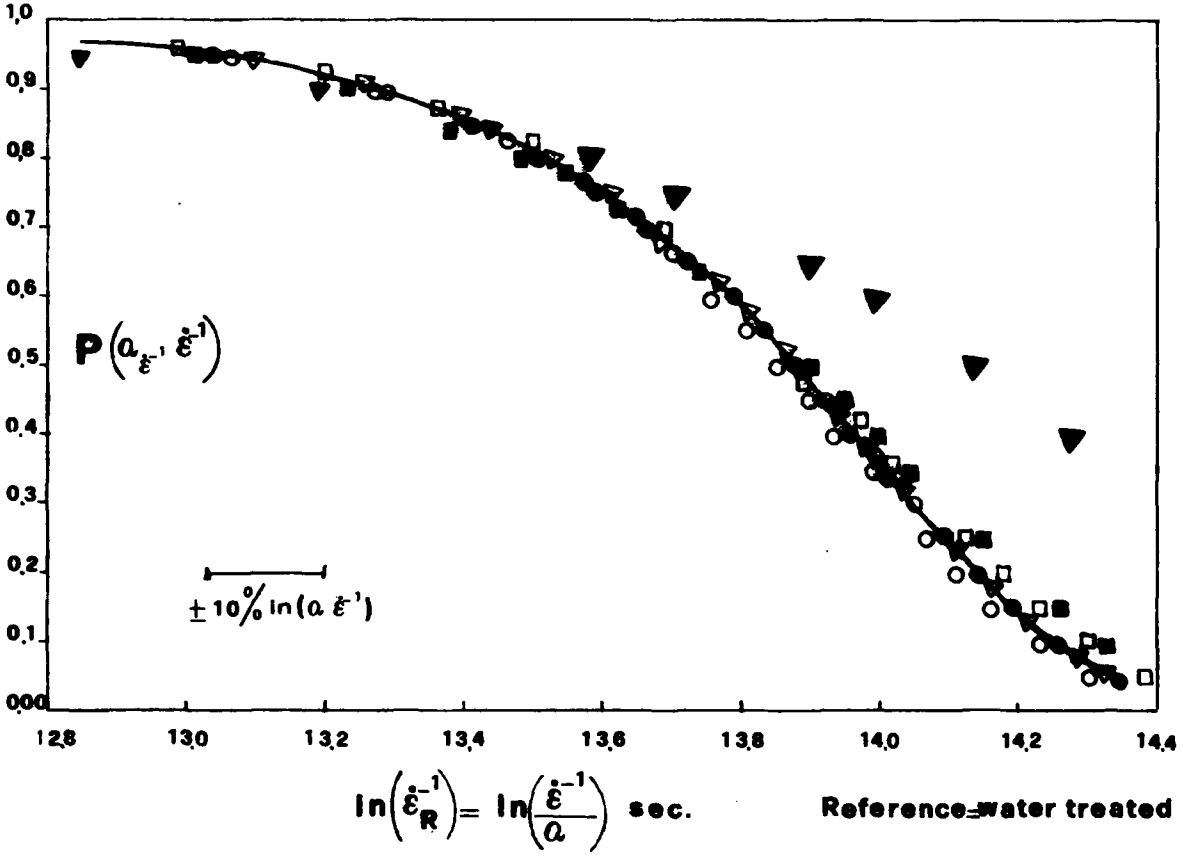

FIG. 14 Master Curve for the Distribution of the Inverse of the Rate of Strain During Fatigue for Water Exposed Composites (Population 4-BW192 at L = 0.7 used as Reference State)

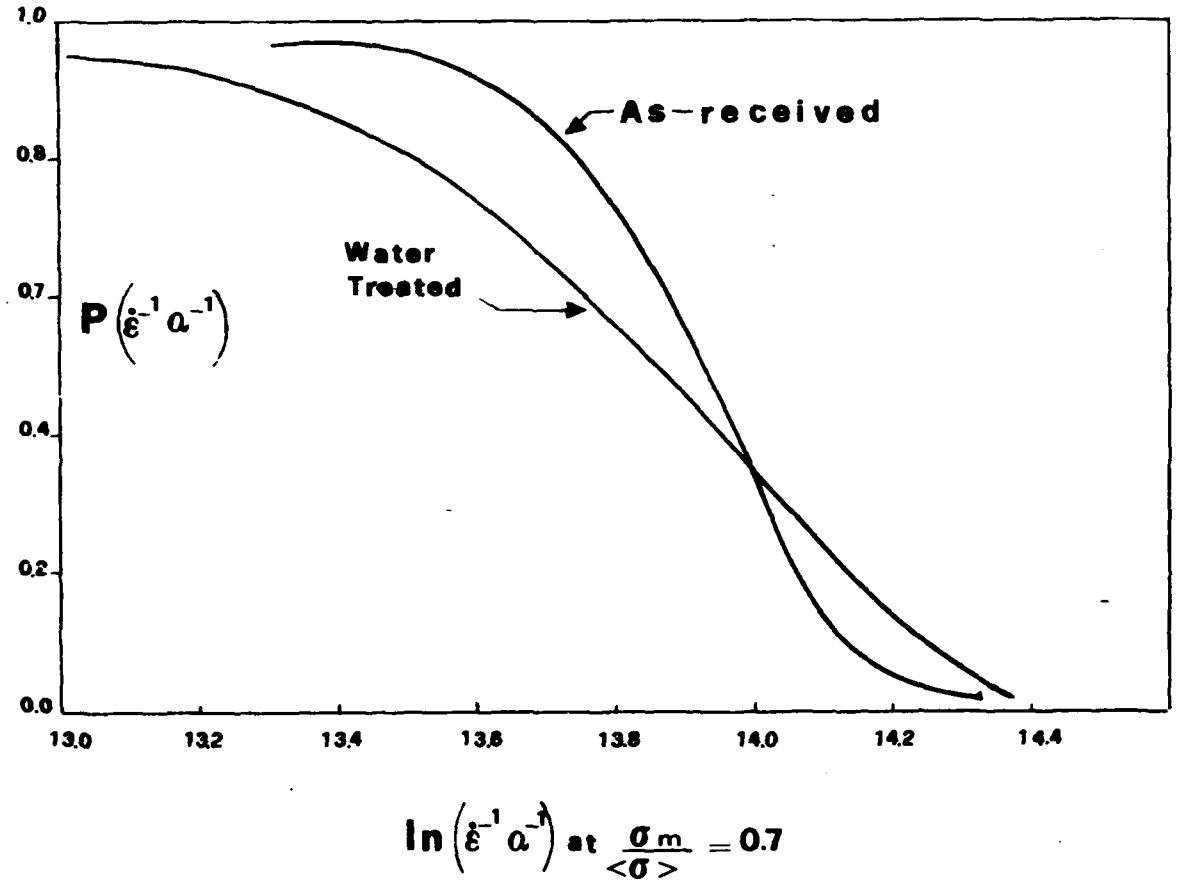

FIG. 15 Comparison of Reduced Plots of the Distributions of the Inverse of the Rates of Strain During Fatigue for As-Received and Water Exposed Composites (Compared at L = 0.7)

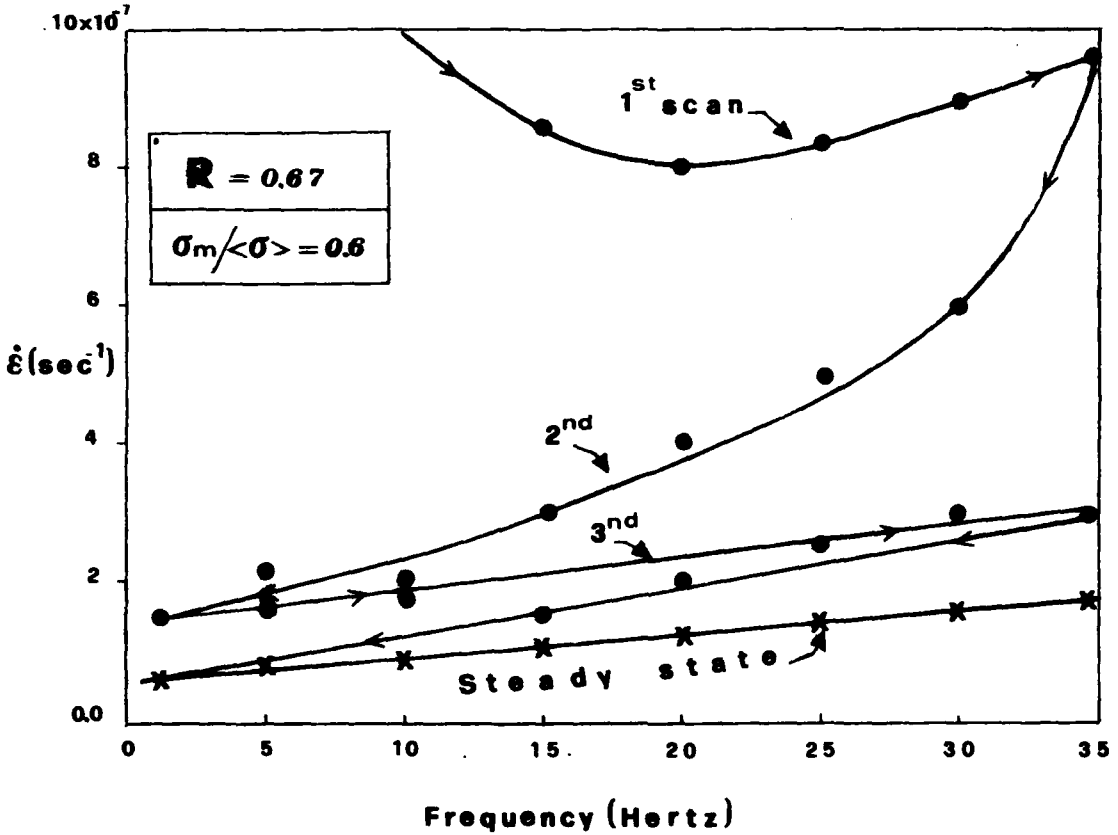

FIG. 16 Effect of Frequency and Time on the Rate of Deformation During Fatigue for a Specimen of Population 2-RH55

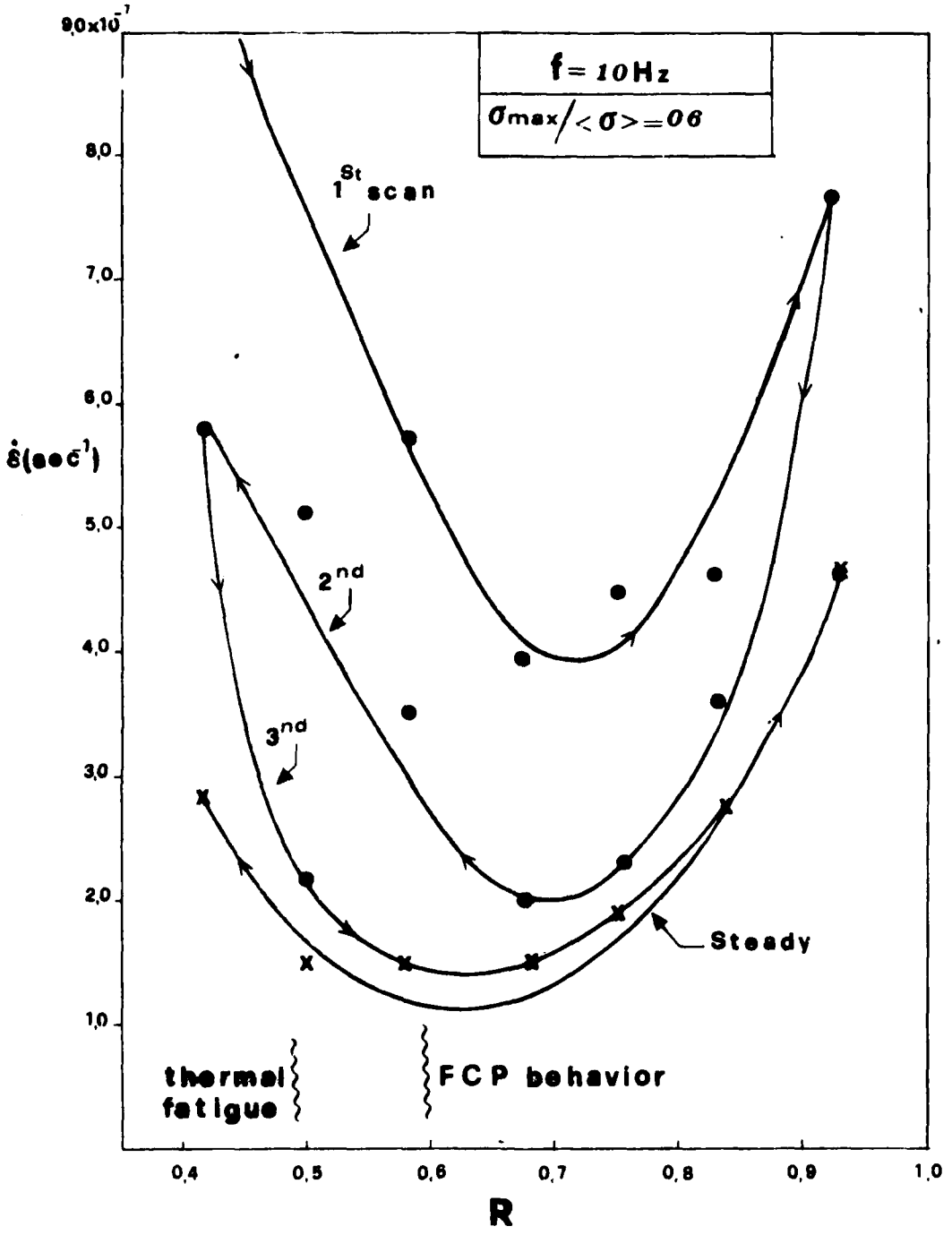

FIG. 17 Effect of Tensile Stress Amplitude and Time on the Rate of Deformation During Fatigue for a Specimen of Population 2-RH55

FIG. 18 Scanning Electron Micrograph of Fracture Surface of Specimen From Population 2-PH55. (Fractured in Ramp Load at 0.2 in/min) ( ) magnification

FIG. 19 Scanning Electron Micrographs of Fracture Surface of Specimen From Population 2-RH55. (Fractured in Fatigue at L = 0.85, R = 2/3 and f = 10 hz)
Upper Photo: Far Edge of Surface 650 mag.
Lower Photo: Near Center of Surface 700 mag.

FIG. 20 Scanning Electron Micrograph of Fracture Surface of Specimen From Population 3-RH100 (Fractured in Ramp Loading at 0.2 in/min) 900 magnification

FIG. 21 Scanning Electron Micrograph of Fracture Surface of Specimen From Population 4-BW192 (Fractured in Fatigue at L = 0.65, R = 2/3, f = 10 hz) 700 magnification

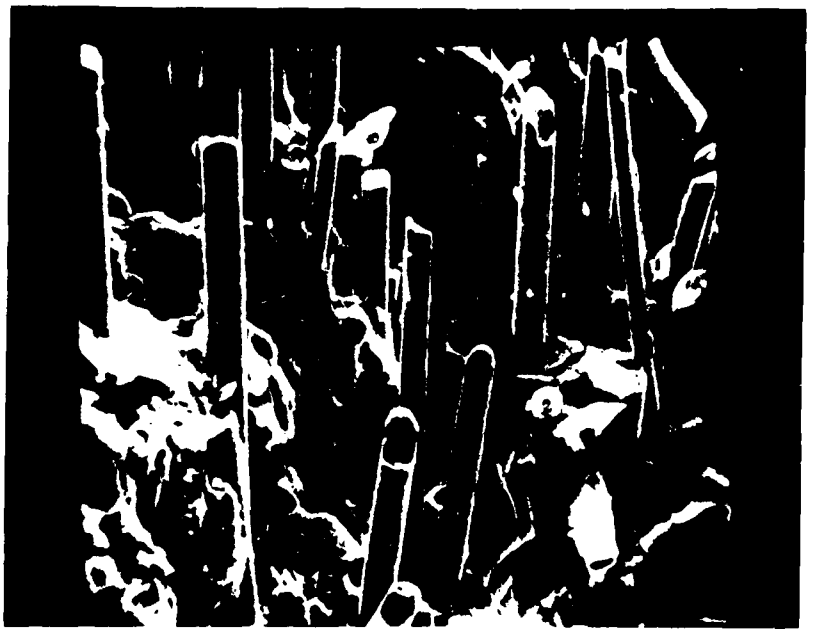

FIG. 22 Scanning Electron Micrograph of Fracture Surface of Specimen From Population 4-BW192 (Fractured in Ramp Loading at 0.2 in/min) 350 magnification

Table 1

Moduli of Elasticity for Glass Fiber Reinforced PBT
(20% by Volume)

Population	Initial Tangent Modulus of Elasticity (psi)
1-RH 55	1,120,000 ± 100,000
2-RH 55	1,050,000 ± 150,000
3-RH 100	970,000 ± 100,000
4-BW 192	940,000 ± 100,000
5-HW 504	990,000 ± 100,000

Table 2

Tensile Properties and Weibull Distribution Parameters

Populations	Strength to Break (psi)				Strain to Break (in/in)				Toughness (lbf/in^2)			
↓	α	σ_o	$\langle\sigma_b\rangle$	r^2	α	ε_o	$\langle\varepsilon_b\rangle$	r^2	α	M_{to}	$\langle M_{tb}\rangle$	r^2
1-RH 55	80.6	17,730	17,609	0.96	20.0	0.033	0.032	0.76	16.9	401	389	0.79
2-RH 55	157.3	17,600	17,540	0.97	16.1	0.030	0.029	0.97	13.7	370	357	0.98
3-RH 100	90.5	16,400	16,300	0.96	32.6	0.034	0.033	0.96	16.1	390	380	0.97
4-BW 192	66.1	11,311	11,221	0.98	14.3	0.016	0.015	0.96	9.7	105	100	0.90
5-HW 504	75.8	14,200	14,100	0.96	17.7	0.021	0.020	0.99	16.2	172	167	0.97

Table 3

Loading Specifications for Cyclic Fatigue Measurements (Stress in psi) f = 10 Hz, R = 2/3

Population	Stress level $L = \sigma_{max}/\langle\sigma_b\rangle$	Max. level $= L \times \langle\sigma_b\rangle$	Mean stress $=(\sigma_{max}+\sigma_{min})/2$	Min. stress $= R \times \sigma_{MAX}$	Stress amplitude $\Delta\sigma=\sigma_{max}-\sigma_{min}$
1-RH 55	0.82	14,435	12,053	9,671	4,764
1-RH 55	0.74	13,030	10,880	8,730	4,300
2-RH 55	0.90	15,789	13,157	10,526	5,263
2-RH 55	0.85	14,912	12,427	9,941	4,971
2-RH 55	0.80	14,032	11,694	9,355	4,677
3-RH 100	0.85	13,855	11,569	9,283	4,572
3-RH 100	0.75	12,225	10,208	8,190	4,035
4-BW 192	0.79	8,863	7,386	5,909	2,954
4-BW 192	0.70	7,853	6,544	5,235	2,618
4-BW 192	0.65	7,292	6,077	4,862	2,430
5-HW 504	0.79	11,139	9,300	7,463	3,676
5-HW 504	0.65	9,165	7,653	6,140	3,025

Table 4

Fatigue Lives and Weibull Distribution Parameters

Populations	Stress level $L = \sigma_{MAX}/\langle\sigma_b\rangle$	α	Time to Break (sec) t_o	$\langle t_b \rangle$	r^2
1-RH 55	0.82	3.16	4,658	4,169	0.98
1-RH 55	0.74	1.95	36,006	31,901	0.94
2-RH 55	0.90	8.65	383	361	0.95
2-RH 55	0.85	5.57	925	854	0.89
2-RH 55	0.80	6.47	1,718	1,600	0.98
3-RH 100	0.85	1.66	5,480	4,877	0.93
3-RH 100	0.75	1.28	63,213	56,170	0.93
4-BW 192	0.79	1.79	656	583	0.97
4-BW 192	0.70	3.40	2,740	2,461	0.92
4-BW 192	0.65	2.44	11,788	10,456	0.92
5-HW 504	0.79	5.99	1,065	988	0.99
5-HW 504	0.65	2.46	29,293	25,983	0.97

Table 5

Examples of Fatigue Strain Data

	Example of Fatigue Strain Data			
σ_{max} psi. / ε_b %	14,912	14,032	8,863	7,853
	0,85<σ>	0,80<σ>	0,79<σ>	0,70<σ>
2,90	0,76 ± 0,20	0,38 ± 0,14		
	1,16 ± 0,20	1,24 ± 0,15		
1,50			0,25 ± 0,08	0,34 ± 0,09
			0,25 ± 0,04	0,23 ± 0,07
Tensile Strain-to-break	Upper No. = ε_I % = cyclic softening strain			
	Lower No. = ε_{II} % = creep-to-break in fatigue			

Table 6

Various Contributions to the Strain-to-Break in Fatigue

Ductility in Tension Test	HIGH $\bar{\varepsilon}_b > 3.3\%$	INTERM. $3.1 > \varepsilon_b > 2.0$	LOW $1.8 > \varepsilon_b > 1.3$
Cyclic Softening $\varepsilon_I\%$	1.0 – 1.6	0.4 – 0.9	0.2 – 0.5
Creep-to-Break in Fatigue $\varepsilon_{II}\%$	0.9 – 1.1	0.6 – 1.4	0.2 – 0.3
Strain-to Break in Fatigue $\varepsilon_{bf}\%$	1.9 – 2.7	1.0 – 2.3	0.4 – 0.8
$\varepsilon_{bf}/\bar{\varepsilon}_b$	0.5 – 0.7	0.4 – 0.6	0.3 – 0.5

Table 7

Loading Values for Stress Ratio Tests

Stress ratio $R=\sigma_{min}/\sigma_{max}$	Frequency (hertz)	Stress level; L = 0.60				Stress level; L = 0.70			
		σ_{max}	σ_{mean}	σ_{min}	$\Delta\sigma$	σ_{max}	σ_{mean}	σ_{min}	$\Delta\sigma$
0.42	10	10,524	7,455	4,385	6,139	12,278	8,697	5,116	7,162
0.50	10	10,524	7,893	5,262	5,262	12,278	9,209	6,139	6,139
0.58	10	10,524	8,332	6,139	4,385	12,278	9,720	7,162	5,116
0.67	10	10,524	8,770	7,016	3,508	12,278	10,232	8,135	4,093
0.75	10	10,524	9,209	7,893	2,631	12,278	10,744	9,209	3,068
0.83	10	10,524	9,647	8,770	1,754	12,278	11,255	10,232	2,046
0.92	10	10,524	10,086	9,647	877	12,278	11,767	11,255	1,023

DISTRIBUTION LIST

No. of Copies	To
1	Office of the Under Secretary of Defense for Research and Engineering, The Pentagon, Washington, D.C. 20301
12	Commander, Defense Technical Information Center, Cameron Station, Building 5, 5010 Duke Street, Alexandria, Virginia 22314
1	Metals and Ceramics Information Center, Battelle Columbus Laboratories, 505 King Avenue, Columbus, Ohio 43201
	Deputy Chief of Staff, Research, Development, and Acquisition, Headquarters, Department of the Army, Washington, D.C. 20310
1	ATTN: DAMA-ARZ
2	Dr. J. I. Bryant
	Commander, Army Research Office, P.O. Box 12211, Research Triangle Park, North Carolina 27709
1	ATTN: Information Processing Office
2	Dr. J. Hurt
1	Dr. G. Mayer
1	Dr. D. Squire
	Commander, U.S. Army Materiel Development and Readiness Command, 5001 Eisenhower Avenue, Alexandria, Virginia 22333
1	ATTN: DRCLDC
	Commander, U.S. Army Armament Research and Development Command, Dover, New Jersey 07801
1	ATTN: Mr. H. Pebly, PLASTEC
1	Mr. A. Slobodzinski, PLASTEC
1	Mr. W. Tanner
	Commander, U.S. Army Natick Research and Development Command, Natick, Massachusetts 01760
1	ATTN: Technical Library
	Commander, U.S. Army Aviation Research and Development Command, P.O. Box 209, St. Louis, Missouri 63166
1	ATTN: Mr. R. Vollmer
	Commander, Harry Diamond Laboratories, 2800 Powder Mill Road, Adelphi, Maryland 20783
1	ATTN: Technical Information Office
	Commander, U.S. Army Foreign Science and Technology Center, 220 7th Street, N.E., Charlottesville, Virginia 22901
1	ATTN: Military Tech, Mr. Marley

No. of Copies	To
	Director, Eustis Directorate, U.S. Army Air Mobility Research and Development Laboratory, Fort Eustis, Virginia 23604
2	ATTN: Mr. W. Figgel
	Chief of Naval Research, Arlington, Virginia 22217
1	ATTN: Code 471
	Office of Naval Research, Boston Branch, 495 Summer Street, Boston, Massachusetts 02210
1	ATTN: Dr. L. H. Peebles
	Naval Research Laboratory, Washington, D.C. 20375
2	ATTN: Dr. W. B. Moniz, Code 6120
2	Dr. I. Woloch, Code 8433
3	Dr. W. D. Bascom, Code 6170
2	Dr. L. B. Lockhart, Jr., Code 6120
	Commander, Naval Air Systems Command, Washington, D.C. 20361
2	ATTN: Mr. C. Bersch
	Commander, Naval Surface Weapons Center, White Oak, Silver Spring, Maryland 20910
1	ATTN: Dr. J. M. Augl
	Air Force Office of Scientific Research (NC), Building 410, Bolling Air Force Base, Washington, D.C. 20332
1	ATTN: Dr. D. R. Ulrich
	Air Force Materials Laboratory, Wright-Patterson Air Force Base, Ohio 45433
1	ATTN: Dr. S. W. Tsai
1	Dr. N. J. Pagano
1	Dr. H. T. Hahn
1	Dr. C. E. Browning
	Air Force Flight Dynamics Laboratory, Wright-Patterson Air Force Base, Ohio 45433
1	ATTN: Dr. G. P. Sendeckyj
	National Aeronautics and Space Administration, Lewis Research Center, 21000 Brookpark Road, Cleveland, Ohio 44135
2	ATTN: Dr. T. T. Serafini (49-1)
1	Dr. C. C. Chamis
1	Professor D. F. Adams, Department of Mechanical Engineering, University of Wyoming, Laramie, Wyoming 82070
1	Professor F. J. McGarry, MIT, Cambridge, Massachusetts 02139

No. of Copies	To
1	Professor K. H. G. Ashbee, University of Bristol, H. H. Wills Physics Lab., Bristol, England BS81TL
1	Professor O. Ishai, Department of Mechanics, Technicon - Israel Institute of Technology, Haifa, Israel
1	Dr. D. H. Kaelble, Science Center, Rockwell International, Thousand Oaks, California 91360
1	Dr. B. W. Rosen, Materials Science Corporation, Blue Bell, Pennsylvania 19422
	Defense Research Establishment Office, Sheelay Bay, Ottawa, Ontario KIA 024
1	ATTN: Mr. H. L. Nash
	Defence Standard Laboratories, Department of Supply, P.O. Box 50, Ascot Vale 3032, Victoria, Australia
1	ATTN: Dr. D. Pinkerton
1	Dr. G. George
	Director, Army Materials and Mechanics Research Center, Watertown, Massachusetts 02172
2	ATTN: DRXMR-PL
1	DRXMR-PR
1	DRXMR-AP
1	DRXMR-PD
4	DRXMR-RC, Mrs. M. Roylance

Army Materials and Mechanics Research Center, AD _____
Watertown, Massachusetts 02172
FATIGUE BEHAVIOR OF GLASS FIBER
REINFORCED POLYBUTYLENETEREPHTHALATE -
A. T. DiBenedetto

Technical Report AMMRC TR 80-17, April 1980,
69 pp - illus-tables
D/A Project 1L162105AH8H
AMCMS Code 62105.11.H8H

UNCLASSIFIED
UNLIMITED DISTRIBUTION

Key Words
Fatigue
Fiber Reinforced Composite
Polybutyleneterephthalate
Environmental tests

The fatigue behavior of short glass fiber reinforced PBT composites was investigated under different environmental conditions. Exposure to water at high temperature caused embrittlement, while improved processing and exposure to high humidity caused an increase in ductility. The quantity $(\sigma_{max}/\langle\sigma\rangle)^2 \ln t_B$ was a unique function of elongation-to-break. The total deformation to break during fatigue consisted of a deformation attributable to cyclic softening and a longer term deformation that continued at nearly constant rate until failure occurred. Crack propagation rates and fatigue life appeared to be dependent on prior stress history.

Army Materials and Mechanics Research Center, AD _____
Watertown, Massachusetts 02172
FATIGUE BEHAVIOR OF GLASS FIBER
REINFORCED POLYBUTYLENETEREPHTHALATE -
A. T. DiBenedetto

Technical Report AMMRC TR 80-17, April 1980
69 pp - illus-tables
D/A Project 1L162105AH8H
AMCMS Code 62105.11.H8H

UNCLASSIFIED
UNLIMITED DISTRIBUTION

Key Words
Fatigue
Fiber Reinforced Composite
Polybutyleneterephthalate
Environmental tests

The fatigue behavior of short glass fiber reinforced PBT composites was investigated under different environmental conditions. Exposure to water at high temperature caused embrittlement, while improved processing and exposure to high humidity caused an increase in ductility. The quantity $(\sigma_{max}/\langle\sigma\rangle)^2 \ln t_B$ was a unique function of elongation-to-break. The total deformation to break during fatigue consisted of a deformation attributable to cyclic softening and a longer term deformation that continued at nearly constant rate until failure occurred. Crack propagation rates and fatigue life appeared to be dependent on prior stress history.

Army Materials and Mechanics Research Center, AD _____
Watertown, Massachusetts 02172
FATIGUE BEHAVIOR OF GLASS FIBER
REINFORCED POLYBUTYLENETEREPHTHALATE -
A. T. DiBenedetto

Technical Report AMMRC TR 80-17, April 1980
69 pp - illus-tables
D/A Project 1L162105AH8H
AMCMS Code 62105.11.H8H

UNCLASSIFIED
UNLIMITED DISTRIBUTION

Key Words
Fatigue
Fiber Reinforced Composite
Polybutyleneterephthalate
Environmental tests

The fatigue behavior of short glass fiber reinforced PBT composites was investigated under different environmental conditions. Exposure to water at high temperature caused embrittlement, while improved processing and exposure to high humidity caused an increase in ductility. The quantity $(\sigma_{max}/\langle\sigma\rangle)^2 \ln t_B$ was a unique function of elongation-to-break. The total deformation to break during fatigue consisted of a deformation attributable to cyclic softening and a longer term deformation that continued at nearly constant rate until failure occurred. Crack propagation rates and fatigue life appeared to be dependent on prior stress history.